International Journal of Nanomedicine

Dovepress
open access to scientific and medical research

Open Access Full Text Article

ORIGINAL RESEARCH

Specific detection of CD133-positive tumor cells with iron oxide nanoparticles labeling using noninvasive molecular magnetic resonance imaging

This article was published in the following Dove Press journal:
International Journal of Nanomedicine
11 November 2015
Number of times this article has been viewed

Ya-Wen Chen[1,2]
Gunn-Guang Liou[3]
Huay-Ben Pan[4,5]
Hui-Hwa Tseng[5,6]
Yu-Ting Hung[4]
Chen-Pin Chou[4,5,7,8]

[1]National Institute of Cancer Research, National Health Research Institutes, Miaoli, [2]Graduate Institute of Basic Medical Science, China Medical University, Taichung, [3]Institute of Molecular and Genomic Medicine, National Health Research Institutes, Miaoli, [4]Department of Radiology, Kaohsiung Veterans General Hospital, Kaohsiung, [5]School of Medicine, National Yang-Ming University, Taipei, [6]Department of Pathology, Kaohsiung Veterans General Hospital, Kaohsiung, [7]Department of Medical Laboratory Sciences and Biotechnology, Fooyin University, Kaohsiung, [8]School of Medicine, National Defense Medical Center, Taipei, Taiwan

Background: The use of ultrasmall superparamagnetic iron oxide (USPIO) nanoparticles to visualize cells has been applied clinically, showing the potential for monitoring cells in vivo with magnetic resonance imaging (MRI). USPIO conjugated with anti-CD133 antibodies (USPIO-CD133 Ab) that recognize the CD133 molecule, a cancer stem cell marker in a variety of cancers, was studied as a novel and potent agent for MRI contrast enhancement of tumor cells.

Materials and methods: Anti-CD133 antibodies were used to conjugate with USPIO via interaction of streptavidin and biotin for in vivo labeling of CD133-positive cells in xenografted tumors and *N*-ethyl-*N*-nitrosourea (ENU)-induced brain tumors. The specific binding of USPIO-CD133 Ab to CD133-positive tumor cells was subsequently detected by Prussian blue staining and MRI with T2-weighted, gradient echo and multiple echo recombined gradient echo images. In addition, the cellular toxicity of USPIO-CD133 Ab was determined by analyzing cell proliferation, apoptosis, and reactive oxygen species production.

Results: USPIO-CD133 Ab specifically recognizes in vitro and labels CD133-positive cells, as validated using Prussian blue staining and MRI. The assays of cell proliferation, apoptosis, and reactive oxygen species production showed no significant differences in tumor cells with or without labeling of USPIO-CD133 Ab. In vivo imaging of CD133-positive cells was demonstrated by intravenous injection of USPIO-CD133 Ab in mice with HT29 xenografted tumors. The MRI of HT29 xenografts showed several clusters of hypotensive regions that correlated with CD133 expression and Prussian blue staining for iron. In rat, brain tumors induced by transplacental ENU mutagenesis, several clusters of hypointensive zones were observed in CD133-expressing brain tumors by MRI and intravenously administered USPIO-CD133 Ab.

Conclusion: Combination of USPIO-CD133 Ab and MRI is valuable in recognizing CD133-expressing tumor cells in vitro, extracellularly labeling for cell tracking and detecting CD133-expressing tumors in xenografted tumors as well as ENU-induced rat brain tumors.

Keywords: MRI, USPIO, CD133, USPIO-CD133 Ab, molecular imaging

Introduction

Cancer stem cells (CSCs) have the ability to give rise to all cell types found in cancer histology.[1,2] CSCs are generally considered to be key contributors to tumor initiation, maintenance, chemoresistance, radioresistance, recurrence, and metastasis.[1,2] CD133 (AC133; human prominin-1), a well-studied stem cell marker, belongs to a family of cell surface glycoproteins harboring five transmembrane domains and is expressed in hematopoietic stem cells and a subset of putative neural stem/precursor cells in the normal adult central nervous system.[3–6] A characteristic feature of CD133 is its rapid

Correspondence: Chen-Pin Chou
Department of Radiology, Kaohsiung Veterans General Hospital, 386, Dazhong 1st Road, Zuoying District, Kaohsiung 813, Taiwan
Tel +886 7 342 2121 ext 6254
Fax +886 7 350 7581
Email r2207759@ms19.hinet.net

down-regulation during cell differentiation, which makes it a unique cell surface marker for identification and isolation of stem cells and progenitor cells in several tissues, such as the endothelium, brain, bone marrow, liver, kidney, prostate, pancreas, and foreskin.[7,8] CD133-positive cells in brain tumors have a capacity for unlimited self-renewal, initiating tumor formation with a small number of cells, and driving tumor progression in xenografts of nude mice.[9,10] CD133 has recently been designated as a marker associated with CSCs or initiating cells in a variety of cancers, such as colon cancer, hepatocellular carcinoma, and glioma tumors.[4,9,11] Furthermore, its prognostic and clinicopathological value in the above-mentioned cancers has been widely studied.[3,12] The recognition of CSCs relies on monoclonal antibody (mAb) against specific antigens on cancer cells. It is very challenging to identify CSCs using conventional clinical imaging scanners, but thus far, in every cancer in which cells have been carefully screened, they have been found.[13,14] The selection of mAb directed at surface antigens expressed by tumor cells has enabled the development of new reagents for diagnostic purposes or for targeted therapies.[15,16]

Magnetic resonance imaging (MRI) is a well-recognized tool for in vivo cell tracking because of its high spatial and contrast resolution, as well as its reproducibility. Combined with an advanced contrast agent, MRI allows for molecular profiling of target tissues/cells and can enable the early detection of malignancies, making more accurate staging and treatment monitoring possible.[17] A number of methods have been developed and refined in experimental models to track and monitor cells in vitro or ex vivo. Nearly all approaches require cell manipulation in vitro. Recently, the use of superparamagnetic iron oxide (SPIO) nanoparticles to visualize cells has been applied clinically, demonstrating the potential to monitor cells in vivo with MRI. SPIO particles consist of ferric (Fe^{3+}) and ferrous (Fe^{2+}) irons. These large magnetic moments result in strong disruptions of the local magnetic field and produce magnetic susceptibility artifacts. Because of this, an important property of SPIO is to improve the contrast enhancement effect by decreasing the T2- and T2*-weighted relation time of tissues and producing a decrease in signal intensity (SI) on magnetic resonance (MR) images. Thus, the signal of MRI is quenched and the presence of SPIO is detected as dark contrast (hypointensity) in MRI.[18–20] The large magnetic moments of SPIO influence the magnetic field beyond the actual size of the particles.[21] SPIO and ultrasmall SPIO (USPIO) are commonly used iron oxide-based contrast agents for cell labeling for this reason. Both the size and the surface-coating material of SPIO particles can affect their pharmacokinetics, inter-organ distribution, and intracellular uptake. In addition, the degree of uptake of the different SPIO products may vary among cancer cell types. Large particles such as SPIO are more easily phagocytosed than small particles such as USPIO.[21] Biologically, USPIO particles have less of a chance for liver uptake, but are small enough to reach the tumor through the capillary wall. The USPIO nanoparticles can stay longer in the circulating blood and are normally taken up by macrophages, including those in lymph nodes and bone marrow.[22] Although the use of SPIO/USPIO is based on a passive targeting mechanism, designed molecular imaging agents can accumulate at a location of disease by active targeting mechanisms. Precise targeting is based on the use of specific ligands (antibodies, peptides, polysaccharides, and drugs), and this approach can be used in the design of ligand-directed, site-specific contrast accumulating agents and other targeted therapies.[23–29]

By labeling CSCs with SPIO/USPIO, the CSC can be identified and tracked in vivo using an MRI scanner, a reliable anatomical and functional assessment of tumor-bearing animals.[30] With the help of SPIO/USPIO-labeling techniques, more studies identifying and characterizing CSCs as well as developing therapeutic treatments can be accomplished. Mediated by the specific recognition of a CSC surface marker, CD133, a novel antibody-functionalized agent in this study, was developed to specifically label CD133-expressing tumor cells in vitro, ex vivo, and in vivo xenografted mice by USPIO conjugated with anti-CD133 antibodies (USPIO-CD133 Ab). Specially, intravenous injection of USPIO-CD133 Ab specifically target CD133-expressing tumor cells in *N*-ethyl-*N*-nitrosourea (ENU)-induced brain tumors in vivo using clinical MRI scanning.

Materials and methods

Ethics statement

This animal study was performed in strict accordance with the recommendations in the guidelines from the Care and Use of Laboratory Animals of Kaohsiung Veterans General Hospital, Taiwan. The protocol was approved by the Institutional Animal Care and Use Committee of Kaohsiung Veterans General Hospital (Protocol number: vghks-99-A037). Animals were kept on a standard rat and mouse diet with free access to tap water and food, with a 12-hour light–dark cycle. All efforts were made to minimize the suffering of animals.

Cell culture

HT29 cells from human colon carcinoma, OC2 cells from human oral cancer,[31] and HepG2 from human hepatoblastoma were grown in the American Type Culture Collection-recommended medium (either Roswell Park Memorial Institute 1640 or high glucose Dulbecco's Modified Eagle's

Medium) (Thermo Fisher Scientific, Waltham, MA, USA) at 37°C in a humidified atmosphere of 95% air and 5% CO_2. All media were supplemented with 1% penicillin/streptomycin (Thermo Fisher Scientific) and 10% fetal bovine serum (Thermo Fisher Scientific).

Conjugation of CD133 Ab with USPIO

The USPIO nanoparticles composed of an Fe_3O_4 core and a dextran coating and USPIO-CD133 Ab were synthesized and obtained from MagQu Co., Ltd (New Taipei, Taiwan) and prepared as described previously.[32–34] Briefly, a ferrite solution containing ferrous sulfate heptahydrate ($FeSO_4 \cdot 7H_2O$) and ferric chloride hexahydrate ($FeCl_3 \cdot 6H_2O$) in a stoichiometric ratio of 1:2 was mixed with an equal volume of aqueous dextran. Dextran was served as a surfactant for Fe_3O_4 particles distributed in water because of its nontoxicity, hydrophilicity, and high affinity for biological macromolecules. The mixture was heated to 70°C–90°C and titrated with a strong base solution to form black Fe_3O_4 particles. Aggregates and excess unbound dextran were removed by centrifugation and gel filtration chromatography to produce a highly homogeneous dextran-coating magnetic nanoparticles. The monoclonal anti-CD133 Ab (ab19898, Abcam, Cambridge, UK) in biotin-labeling buffer was mixed with *N*-hydroxysuccinimide ester biotin (10 µL of 10 mg/mL in dimethyl sulfoxide Sigma-Aldrich, St Louis, MO, USA) and then incubated for 90 minutes at room temperature. After removing unbound biotin by dialysis, biotinylated anti-CD133 Ab (25 µg/50 µL) was bound to USPIO (1 mL of lyophilized USPIO agent powder/30 mL of phosphate-buffered saline [PBS], MagQu Co., Ltd) particles with coating streptavdin on dextran. Followed by magnetic separation to remove unbound biotinyl-anti-CD133, USPIO-CD133 Ab via interaction of streptavdin and biotin was obtained. The morphology of antibody-functionalized USPIO was round in shape as described previously.[35] The magnetic hysteresis of USPIO-CD133 Ab was detected by using a vibrating sample magnetometer (HysterMag, MagQu Co., Ltd). According to the magnetic hysteretic curve, USPIO-CD133 Ab showed superparamagnetism. The antibody-functionalized USPIO was stable at least for 6 months as stored at 2°C–8°C as shown previously.[36–38]

Detection of nanoparticles by transmission electron microscopy

The negative staining of electron microscope sample was described previously with some modifications.[39] Briefly, one drop of nanoparticles was adsorbed to a glow-discharged 200-mesh copper grid covered with carbon-coated collodion film, washed with three drops of distilled water, and then stained with two drops of 0.75% uranyl acetate (Sigma-Aldrich). The samples were examined and photographed with an FEI Tecnai G2 spirit (FEI, Hillsboro, OR, USA) or a Hitachi H7650 EM (Hitachi, Berkshire, UK).

Prussian blue staining

Cells were fixed with 4% paraformaldehyde (Sigma-Aldrich) for 15 minutes and washed with distilled water twice. Fixed cells were incubated for 20–30 minutes with a mixing solution of 2% potassium ferrocyanide (Sigma-Aldrich) and 6% hydrogen chloride (Sigma-Aldrich), then washed twice with PBS and finally counterstained for 30 seconds with nuclear fast red (Sigma-Aldrich). The de-waxed sections were stained by mixing of hydrochloric acid and potassium ferrocyanide prepared immediately before use and immersed in the solution. Slides were washed in distilled water, counterstained and then dehydrated using serial grading alcohol and xylene. Cells or slides were finally covered with mounting medium and observed under a light-field microscope.

Cell proliferation assay

One thousand cells labeled with nanoparticles for 4 hours were implanted into 96-well plate and quantified their growth by using CellTiter 96 Aqueous Non-Radioactive Cell Proliferation assay (Promega Corporation, Fitchburg, WI, USA) for 3 days according to the manufacturer's instructions. The absorbance was measured at a wavelength of 490 nm.

Cell apoptosis assay

Cells labeled with nanoparticles for 4 hours were collected after trypsinization, and re-suspended in PBS at 10^6 cells/mL. According to the manufacturer's instructions, fluorescent-labeled Annexin V medium and propidium iodide/7-aminoactinomycin D (FITC/PE Annexin V Apoptosis Detection Kits, BD Biosciences, San Jose, CA, USA) were added to cell suspension, which was kept at room temperature for 15–20 minutes. The percentages of dead cells and cells undergoing apoptosis were determined using a flow cytometer (FACS Calibur, BD Biosciences).

Measurement of reactive oxygen specie

Intracellular reactive oxygen species (ROS) levels of cells labeled with nanoparticles for 4 hours were measured by a fluorescence microscope (Olympus LX71 microscope, Olympus Corporation, Tokyo, Japan) and a flow cytometer

using 50 μM of CM-H_2DCFDA (5-(and-6)-chloromethyl-2′,7′-dichlorodihydrofluorescein diacetate) (Thermo Fisher Scientific) as the fluorescent probe according to the previous study.[40]

Preparing USPIO-CD133 Ab-labeled cells for MRI

Two in vitro MRI phantoms with cylindrical plastic containers and agarose gel bed were made for USPIO-CD133 Ab medium and USPIO-CD133 Ab-labeled cells. The first phantom contained eight test tubes of USPIO-CD133 Ab medium diluted using PBS with different concentrations (0.078, 0.156, 0.312, 0.625, 1.25, 2.5, 5, and 10 μg/mL free iron) placed in gel bed. The second phantom contained eight vials of 10^3 cells labeling with different concentrations of USPIO-CD133 Ab. 5×10^4 $CD133^+$ cells were seeded onto each well of the 6-well plates with labeling agent USPIO-CD133 Ab at different concentrations equivalent to 0, 10, 20, 40, 80, and 100 mg/mL USPIOs at 37°C for 1 hour. The culture medium was then washed with PBS three times; the cells were trypsinized and counted. One thousand USPIO-CD133 Ab-labeled cells were placed and fixed in 4% formaldehyde in test tubes (1.5 mL) with PBS separately. After centrifugation at 4,000 rpm for 5 minutes, the test tubes with cellular pellet were placed in gel bed. The areas of signal void on MRI were visualized in the test tubes due to USPIO-CD133 Ab and USPIO-CD133 Ab nanoparticle-labeled cell pellets.

Pre-labeling with USPIO-CD133 Ab for subcutaneous xenografts

One million HT29 cells were incubated with USPIO-CD133 Ab nanoparticles (100 μg Fe/mL) for 4 hours and then subcutaneously injected into target areas of 3–4 male immunocompromised mice with the age of 5–6-week-old (National Laboratory Animal Center, Taipei, Taiwan). Waiting 2–3 weeks for adequate tumor growth, the mice were brought to the MRI scanner.

In vivo labeling USPIO-CD133 Ab for subcutaneous xenografts

One hundred thousand $CD133^{high}$ and $CD133^{low}$ HT29 cells were separately injected into bilateral flanks of 3–4 nude mice and grown until the tumor sizes reached an adequate tumor growth. Images of tumor xenografts were taken before and after intravenously administrated USPIO-CD133 Ab nanoparticles.

MR imaging of cells and animals

MRI of cell pellet and tumor-bearing animals were performed at a clinical 1.5T MRI (Signa, GE Medical Systems, Milwaukee, WI, USA) and an 8-channel phased-array wrist coil. All images were obtained as follows: axial 2D fast spin echo (FSE) sequence (time to echo [TE]/time to repetition [TR] =6,000/99; number of excitations [NEX] =8; echo train length =32; array spatial sensitivity encoding technique =2) and an axial T2-weighted gradient-echo (GRE) sequences (TR/TE =300/20, flip angle =20°, NEX =2) and multiple echo recombined gradient echo (Merge) sequence (TR/TE =950–1,013/3–16, NEX =2). The matrix was 192–256×192, field of view was 70×70 mm, and section thickness was 2 mm. Tumor cells were fixed in 4% paraformaldehyde. After anesthetizing by isoflurane (Baxter International Inc., Deerfield, IL, USA), the animals were placed prone in a wrist coil to get axial images of target-implanted tumor area. After the scan, animals were sacrificed and tissues were fixed in formalin for the subsequent processing. A baseline image of tumor-bearing mice was acquired before USPIO-CD133 Ab nanoparticles intravenously injected. After intravenous injection of nanoparticles (10 mg Fe/kg), the animals were scanned repeatedly at the multiple time points of 1, 2, 24, and 48 hours by MRI. The signal intensities of the nanoparticle-CD133 Ab-labeled cells were determined from a circular region of interest. The size of region of interest depended on the size of the hypointensive area on the images The percentage change in SI (ΔSI) due to labeling was defined as follows: $\Delta SI = [(SI_L - SI_U)/SI_U] \times 100\%$, where SI_L is the signal intensity of the USPIO-labeled cells and SI_U is the signal intensity of the unlabeled control cells. All analyses were performed by the consensus of two experienced MRI radiologists.

Immunohistochemistry

The immunohistochemistry (IHC) was conducted as described previously.[41] Briefly, the de-waxed sections were heated in a microwave for 20 minutes in a citrate buffer (pH 6.0) and incubated with 3% hydrogen peroxide (Sigma-Aldrich) to block the endogenous activity. The samples were individually allowed to react with primary antibodies as follows: anti-CD133 (ab19898, Abcam) and anti-CD68 (ab31630, Abcam). After several washes, horseradish peroxidase/Fab polymer conjugate (Polymer Detection System, Thermo Fisher Scientific) was then applied to the sections, and the sections were incubated for 10 minutes. After rinsing with PBS, the sections were incubated with peroxidase substrate diaminobenzidine (1:20 dilution, Thermo Fisher Scientific) for 5 minutes and counterstained with hematoxylin for 2 seconds, dehydrated with serial alcohol, cleared with xylene, and finally mounted. All illustrations were composed using Adobe Photoshop software (version 6.0, Adobe Systems, Incorporated, San Jose, CA, USA), adjusting only brightness and contrast for optimal visualization.

ENU-induced rat brain tumors

Pregnant female Sprague Dawley rats were purchased from the National Laboratory Animal Center (Taipei, Taiwan) and intraperitoneally injected ENU (50 mg/kg, Sigma-Aldrich) on day 18 of gestation as described previously.[42,43] All offspring were screened at the age of 3 months to monitor the tumor formation and growth by MRI. Before injecting USPIO-CD133 Ab nanoparticles, baseline images of three to four tumor-bearing animals were acquired. After intravenous injection of nanoparticles (10 mg Fe/kg), the anesthetized animals were brought to 1.5T MRI scanner at the time points of 1, 2, 24, and 48 hours for MRI scan. After the scan, animals were sacrificed and tissues were fixed in formalin for the subsequent processing.

Immunofluorescence

Cells plated on the coverslips or slide chambers were fixed with 4% paraformaldehyde, permeabilized with 0.1% Triton X-100 (Sigma-Aldrich)/PBS, and incubated with primary antibody, followed by intensive washes and appropriate secondary antibodies conjugated with fluorescent dyes and finally viewed under a fluorescent microscope. Primary antibodies were used as below: anti-CD133 (ab19898, Abcam), anti-CD68 (ab31630, Abcam), and anti-oligodendrocyte specific protein (ab53041, Abcam).

Statistical analysis

Each experiment was repeated at least twice. Statistical analysis was performed using GraphPad software (GraphPad Software, Inc., La Jolla, CA, USA). The data were expressed as means ± standard error of the mean. A difference with $P<0.05$ was considered statistically significant.

Results

In vitro detection of USPIO-CD133 Ab binding to HT29 cells by MRI

The conjugation of CD133 antibody with nanoparticles, composed of an Fe_3O_4 core and a dextran coating, was accomplished by the binding of USPIO with streptavidin and of anti-CD133 antibodies with biotin. Images by transmission electron microscopy showed various sizes of nanoparticles distributed in populations of both USPIO and USPIO-CD133 Ab (Figure 1A). The average size of USPIO-CD133 Ab nanoparticles was estimated at 29.4±7.9 nm, as compared to USPIO nanoparticles with an average size of 22.9±6.8 nm (Figure 1B).

HT29 human colon cancer cells have been previously reported to contain a high proportion of CD133-positive cells in the total population.[44] By immunofluorescence staining, HT29 cells showed positive expression of CD133 on cell surfaces (Figure S1A). Using flow cytometric analysis, the percentage of CD133-positive HT29 cells was determined to

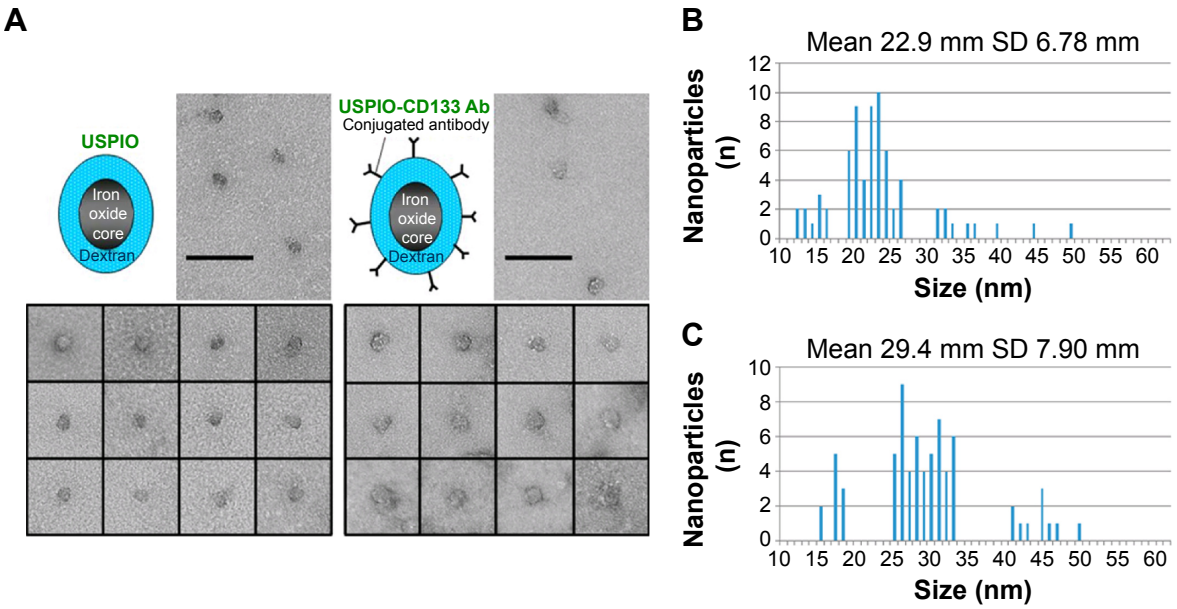

Figure 1 Conjugation of CD133 antibodies with ultrasmall superparamagnetic iron oxides (USPIO-CD133 Ab).
Notes: (**A**) The distribution of USPIO and USPIO-CD133 Ab nanoparticles was observed by transmission electron microscopy. Bar, 100 nm. Spectrum histograms of the sizes of USPIO (**B**) and USPIO-CD133 Ab (**C**) are shown.
Abbreviations: USPIO, ultrasmall superparamagnetic iron oxide; USPIO-CD133 Ab, USPIO conjugated with anti-CD133 antibodies.

be 73.5% of the population (Figure S1B). Results indicated that HT29 cells would be an appropriate in vitro system to evaluate the binding specificity of USPIO-CD133 Ab. To assess the binding capability, USPIO-CD133 Ab but not USPIO binding to HT29 cells was demonstrated by Prussian blue staining (Figure 2A). In contrast, smooth muscle cells that served as negative controls did not show USPIO-CD133 Ab labeling (Figure 2A). Additionally, Prussian blue staining did not show USPIO-CD133 Ab binding to HepG2 (human hepatoblastoma cells) or to OC2 cells (oral squamous cell carcinoma cells), both of which showed low levels of CD133 protein expression by Western blotting (Figure S2). To evaluate the potential for in vitro detection of USPIO-CD133 Ab binding to CD133-positive cells by MRI, eight standard samples with iron concentrations ranging from 0 to 100 μg Fe/mL were prepared by diluting the commercially

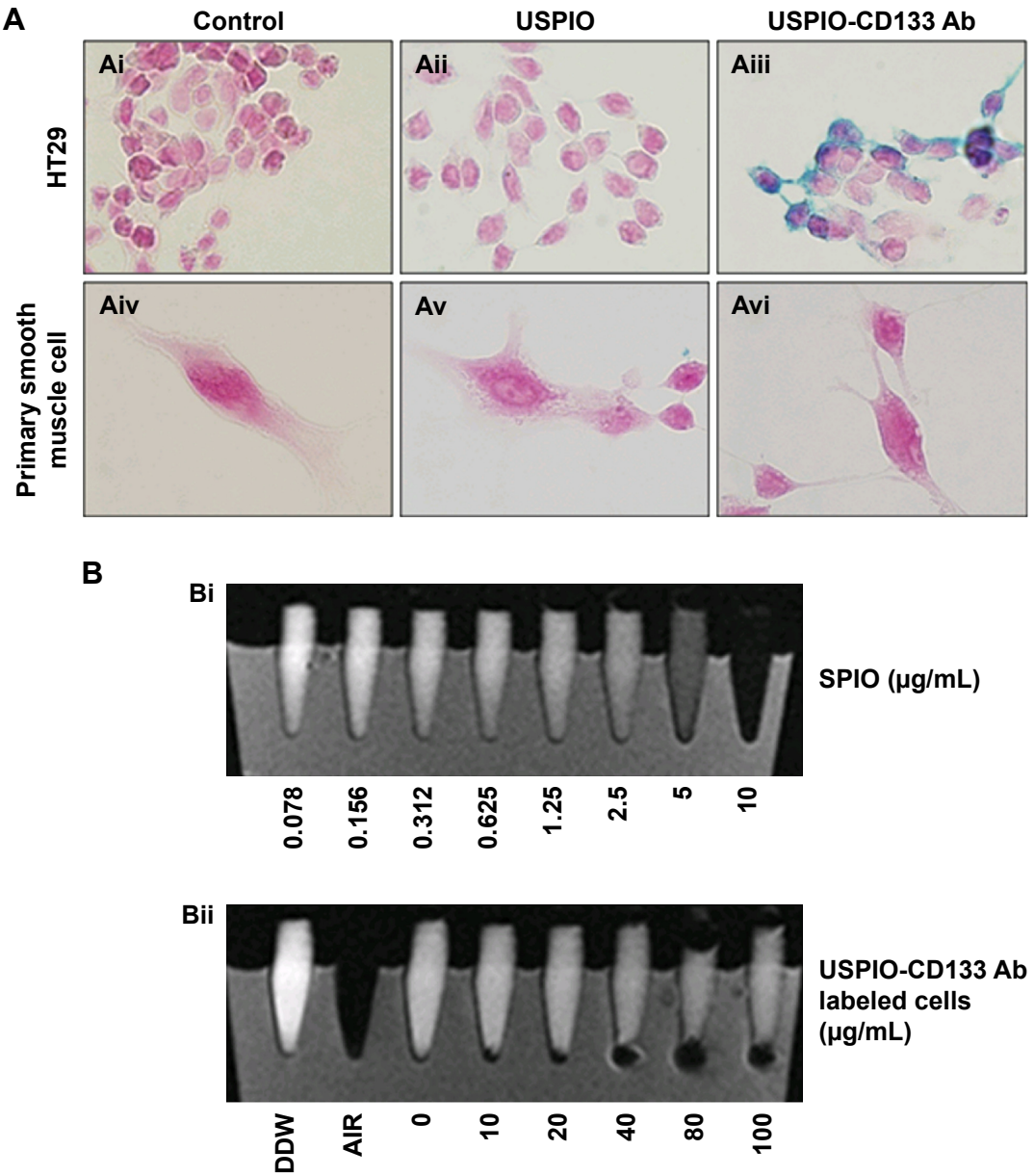

Figure 2 In vitro detection of USPIO-CD133 Ab binding to HT29 cells.

Notes: (**A**) The binding of USPIO-CD133 Ab was examined by Prussian blue staining in HT29 cells incubated with PBS (control), USPIO, and USPIO-CD133 Ab (**Ai**–**Aiii**). Smooth muscle cells with negative CD133 expression served as negative controls, and were incubated with PBS, USPIO, and USPIO-CD133 Ab (**Aiv**–**Avi**). Images were obtained under light-field microscope with 1,000× magnification. (**B**) In vitro MRI cell imaging of iron concentrations in standards and in USPIO-CD133 Ab-labeled cells. (**Bi**) Signals of T2-weighted fast spin echo (FSE) images from serial dilutions of a known concentration of SPIO (Resovist). (**Bii**) T2-weighted FSE images showing different concentrations (0 to 100 μg Fe/mL) of extracellular labeling after the incubation of USPIO-CD133 Ab with HT29 cells. Distilled water (DDW) or empty tube (AIR) served as references.

Abbreviations: MRI, magnetic resonance imaging; PBS, phosphate-buffered saline; SPIO, superparamagnetic iron oxide; USPIO, ultrasmall SPIO; USPIO-CD133 Ab, USPIO conjugated with anti-CD133 antibodies.

available SPIO (Resovist), and were imaged by a 1.5T GE MRI scanner and 8-channel wrist coil. The images for measuring the iron concentration in serial dilutions were acquired using a T2-weighted FSE sequence. Results demonstrated that a decreasing T2 signal was observed with increasing concentrations of SPIO in a dose-dependent manner (Figure 2B). To estimate the amount of USPIO-CD133 Ab in the labeled CD1330-positive tumor cells, MRI of spin-down cells with different concentrations of USPIO-CD133 Ab labeling were analyzed. Similar to the signals detected from diluted SPIO, the cells labeled with USPIO-CD133 Ab showed gradually decreasing SI that correlated with increasing concentrations of USPIO-CD133 Ab (Figure 2B). These results indicated that specific binding between USPIO-CD133 Ab and CD133-positive tumor cells in vitro could be detected by MRI.

Cellular toxicity of USPIO-CD133 Ab

To investigate whether USPIO-CD133 Ab has any cytotoxic effects on HT29 cells, cell growth was analyzed using the 3-(4,5-dimethylthiazol-2-yl)-5-(3-carboxymethoxyphenyl)-2-(4-sulfophenyl)-2H-tetrazolium (MTS) assay. There was no significant change in the proliferation of HT29 cells after in vitro labeling with high- or low-dose USPIO-CD133 Ab when compared with cells incubated either with USPIO alone or untreated (Figure 3A). Similarly, growth of HepG2 and OC2 cells did not show any change after incubation with USPIO alone or with different concentrations of USPIO-CD133 Ab (20 and 100 μg/mL) (Figure S3). Furthermore, whether cell apoptosis occurred after incubation with different labeling reagents was studied. On staining with Annexin V/7-aminoactinomycin D, no increase was found in the late apoptotic incidence between cells labeled with USPIO (2.6%) and the untreated control cells (3.3% in Figure S4A). Stained by Annexin V/PI, four groups of treated cells, including HT29 cells without treatment (control), HT29 cells treated with H_2O_2 (positive control), and HT29 cells incubated with different concentrations of USPIO-CD133 Ab were investigated. High percentage (14.1%) of apoptotic incidence was detected in HT29 cells with H_2O_2 treatment. However, no apparent difference in apoptotic incidence was observed after 20 (6.6%) and 100 μg/mL (7.4%) of USPIO-CD133 Ab labeling when compared with the untreated control (6.1%) (Figure S4B). The relative percentage of apoptotic cells in HT29 cells treated with H_2O_2 was twofold higher than that in HT29 cells without treatment or with USPIO-CD133 Ab treatment (Figure 3B), indicating that there is no effect on apoptotic incidence when cells were treated with USPIO-CD133 Ab.

The cytotoxicity of nanoparticles commonly arises from the production of excess ROS, including free radicals such as the superoxide anion, hydroxyl radicals, and the nonradical hydrogen peroxide.[45,46] The intracellular formation of ROS in HT29 cells incubated with or without USPIO-CD133 Ab was detected using the fluorescent probe CM-H_2DCFDA. Quantification of ROS production was determined using flow cytometry and observation by immunofluorescence microscopy (Figure 3C). The positive signal in HT29 cells treated with H_2O_2 was 27%; however, there was no apparent signal in HT29 cells without treatment (0.5%) or with USPIO-CD133 Ab treatment (0.4% for 20 μg/mL and 0.5% for 100 μg/mL) (Figure 3C). This result demonstrated that the levels of nanoparticle-induced intracellular ROS production were low in USPIO-CD133 Ab-labeled HT29 cells and similar to levels in untreated cells (Figure 3C).

Ex vivo labeling of USPIO-CD133 Ab

HT29 cells ex vivo labeled with USPIO-CD133 Ab were injected subcutaneously into both flanks of immunocompromised mice. Detected by MRI scanning on day 14 after injection, the USPIO-CD133 Ab-labeled tumors showed several clusters of hypointensive regions on FSE T2-weighted images (Figure 4A). The signal ratios of xenograft/muscle were 6.9±0.7 and 0.36±0.04 in unlabeled and labeled tumor cells, respectively ($P<0.05$, Figure 4B). On Merge scans, a prominent signal loss was consistently noted due to the magnetic susceptibility artifact of USPIO ($P<0.05$) (Figure 4A). The representative signal ratios of xenograft/muscle were 1.3±0.05 and 0.21±0.01 in HT29 xenografts without or with ex vivo labeling of USPIO-CD133 Ab, respectively (Figure 4B).

In vivo labeling of USPIO-CD133 Ab in CD133-positive subcutaneous xenografts

To investigate in vivo labeling efficiency of USPIO-CD133 Ab, intravenous injection of USPIO-CD133 Ab was applied in the mouse xenograft models of HT29 cells. FSE T2-weighted MRI showed an apparent decrease in SI of xenografted tumors after intravenous injection of USPIO-CD133 Ab into mice (Figure S5). Furthermore, to determine whether USPIO-CD133 Ab could be differentially delivered to $CD133^{high}$ and $CD133^{low}$ HT29 xenografts, HT29 xenografts with high and low expression of CD133 were established after subcutaneous injection of fluorescence-activated cell sorting-sorted $CD133^{high}$ and $CD133^{low}$ HT29 cells into nude mice (Figure 5A). The pathology and CD133 expression of xenografted tumors were examined by hematoxylin and eosin staining and CD133 immunostaining

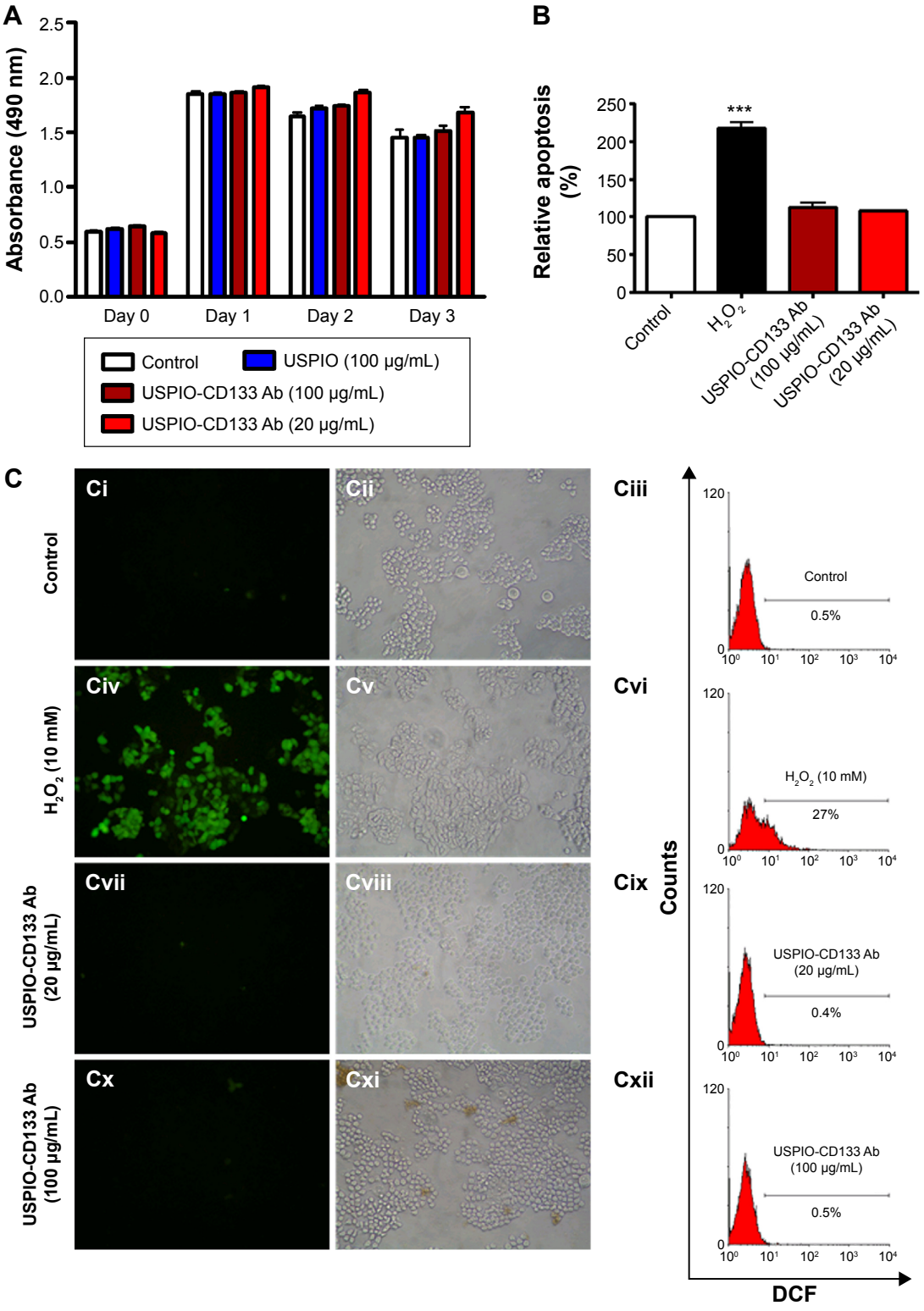

Figure 3 USPIO-CD133 Ab does not show in vitro cell toxicity.

Notes: (**A**) No significant difference in cells growth was detected between USPIO-CD133 Ab-labeled and unlabeled HT29 cells analyzed by MTS assay. (**B**) No apparent difference in cell apoptosis was found between USPIO-CD133 Ab-labeled and unlabeled HT29 cells analyzed by propidium iodide (PI) and Annexin V staining. The relative percentage of apoptosis was obtained by normalizing the mean of the apoptosis percentages in HT29 cells treated by H_2O_2 or USPIO-CD133 Ab relative to percentages in control cells. Bar, SE; ***$P<0.001$. (**C**) No significant difference in ROS production was observed between USPIO-CD133 Ab-labeled and unlabeled HT-29 cells analyzed by DCFDA staining. Detection of ROS in untreated HT-29 cells (**Ci**–**Ciii**); HT29 treated with H_2O_2 (**Civ**–**Cvi**); HT29 treated with USPIO-CD133 Ab at 20 μg/mL (**Cvii**–**Cix**); and HT29 treated with USPIO-CD133 Ab at 100 μg/mL (**Cx**–**Cxii**) using a fluorescent microscope (**Ci**, **Civ**, **Cvii**, **Cx**) and a flow cytometer (**Ciii**, **Cvi**, **Cix** and **Cxii**). DCF (fluorescence) is the end product after CM-H_2DCFDA (no fluorescence) reacted with ROS.

Abbreviations: CM-H_2DCFDA, 5-(and-6)-chloromethyl-2′,7′-dichlorodihydrofluorescein diacetate; DCF, dichlorohydrofluorescein; MTS, 3-(4,5-dimethylthiazol-2-yl)-5-(3-carboxymethoxyphenyl)-2-(4-sulfophenyl)-2H-tetrazolium; ROS, reactive oxygen species; SE, standard error of the mean; USPIO, ultrasmall superparamagnetic iron oxide; USPIO-CD133 Ab, USPIO conjugated with anti-CD133 antibodies.

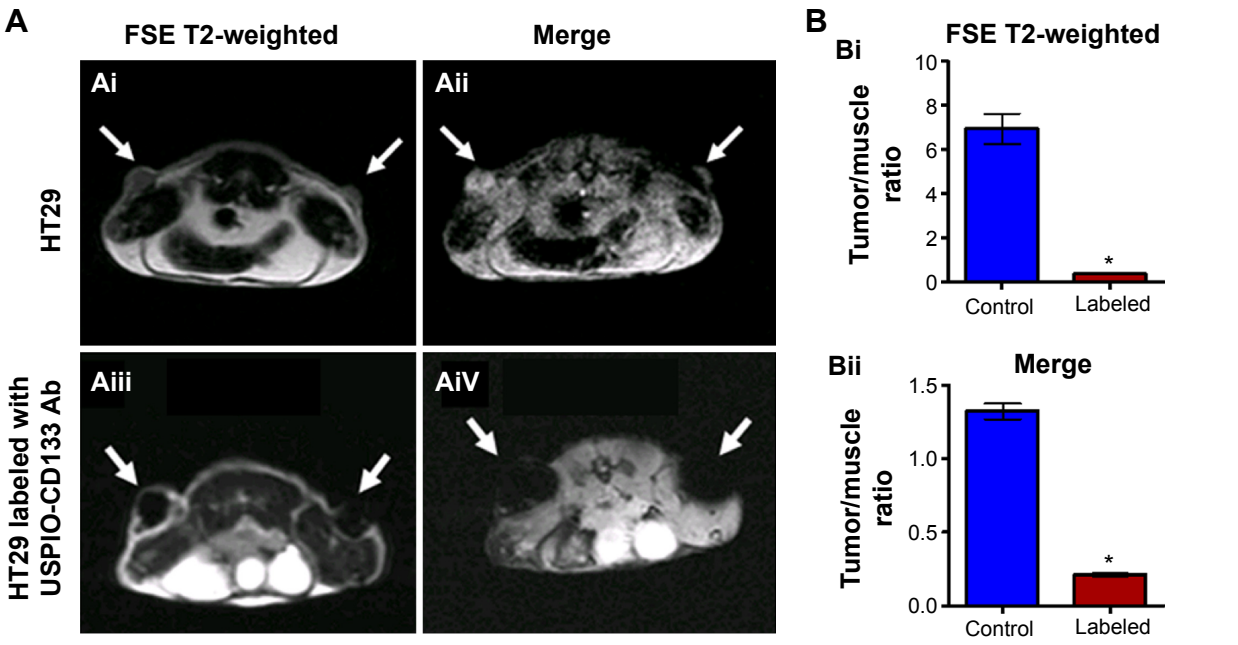

Figure 4 Detection of tumors by MRI in nude mice implanted with HT29 cells ex vivo labeled with USPIO-CD133 Ab.
Notes: (**A**) On day 14 after subcutaneous injection of HT29 cells without (**Ai** and **Aii**) or with ex vivo labeling of USPIO-CD133 Ab (**Aiii** and **Aiv**), xenografted tumors were noted at both flanks (arrows) and scanned by MRI for FSE T2-weighted (**Ai** and **Aiii**) and Merge (**Aii** and **Aiv**) images. (**B**) The representative signal ratio of tumor/muscle in MR images, including FSE T2-weighted (**Bi**) and Merge images (**Bii**). Bar, SE; *$P<0.05$.
Abbreviations: FSE, fast spin echo; MRI, magnetic resonance imgaing; Merge, multiple echo recombined gradient echo; SE, standard error of the mean; USPIO-CD133 Ab, ultrasmall superparamagnetic iron oxide conjugated with anti-CD133 antibodies.

(Figure 5A). After USPIO-CD133 Ab was intravenously injected, the GRE and Merge images showed decreased SI in $CD133^{high}$ xenografted tumors relative to $CD133^{low}$ tumors (Figure 5B and C). The representative signal drop ratios in GRE images between pre- and postinjection were 23.5%±9.5% and 69%±1% in $CD133^{low}$ and $CD133^{high}$ xenografts, respectively, showing a significant difference (P=0.0414) in label detection between CD133 expression levels. The representative signal drop ratios on Merge images between pre- and postinjection were 17%±7% and 66.5%±8.5% in $CD133^{low}$ and $CD133^{high}$ xenografts, respectively, also demonstrating a significant difference (P=0.0461) between xenograft types. Similarly, the GRE and Merge images showed less SI in HT29 xenograft tumors than in HepG2 tumors after intravenous injection of USPIO-CD133 Ab (Figure S6). Additionally, more USPIO-CD133 Ab nanoparticles were observed by Prussian blue staining in $CD133^{high}$ tumor specimens than in $CD133^{low}$ tumor specimens (Figure 5D). These results suggested that USPIO-CD133 Ab could differentially label $CD133^{high}$ tumors in vivo for detection by the MRI.

In vivo labeling of USPIO-CD133 Ab in ENU-induced rat brain tumors

To assess whether USPIO-CD133 Ab can specifically target chemical-induced tumor cells in vivo and be monitored by MRI, USPIO-CD133 Ab was injected into rat brain tumor models established by transplacental ENU mutagenesis. Pregnant female Sprague Dawley rats were intraperitoneally injected with ENU on day 18 of gestation. All of the offspring were screened by MRI beginning at the age of 3 months to monitor tumor growth. ENU-induced intracranial cerebral tumors were first observed on T2-weighted images and showed CD133 expression by IHC in diseased brain sections (Figure S7). After detection of brain tumor formation in rats, USPIO-CD133 Ab was intravenously injected into the animals, and they were scanned in vivo by MRI. In comparison with the MR images in preinjection tumor masses, MR images, including FSE T2-weighted, GRE, and Merge images, showed an apparent decrease in SI after USPIO-CD133 Ab injection (Figure 6A). To confirm the relationship between the decrease in MRI signals and the binding of USPIO-CD133 Ab in tumor specimens, the iron levels were evaluated by Prussian blue staining. The data demonstrated that the cells with significant Prussian blue staining were located in the brain tumors in which MRI signals were decreased after USPIO-CD133 Ab injection (Figure 6B). After grouping by CD133 expression levels using IHC, the signal drop ratios in GRE images were 20.7%±9.7% and 67.7%±4.8% in weak and strong CD133-expressing ENU-induced brain tumors, respectively, demonstrating a

significant difference (P=0.0357). In addition, the signal drop ratios in Merge images also showed a significant difference between the two groups with weak and strong CD133 expression (P=0.0305, Figure 6C).

To further investigate which cells were labeled with USPIO-CD133 Ab in ENU-induced brain tumors, different glial cells were examined in brain tumor sections by immunofluorescence staining with anti-CD133, anti-CD68, and anti-oligodendrocyte specific protein antibodies. Our data indicated that CD133 was highly expressed in oligodendrocytes but not in microglial cells (Figure 7A). Results demonstrated by IHC with anti-CD133 and Prussian blue

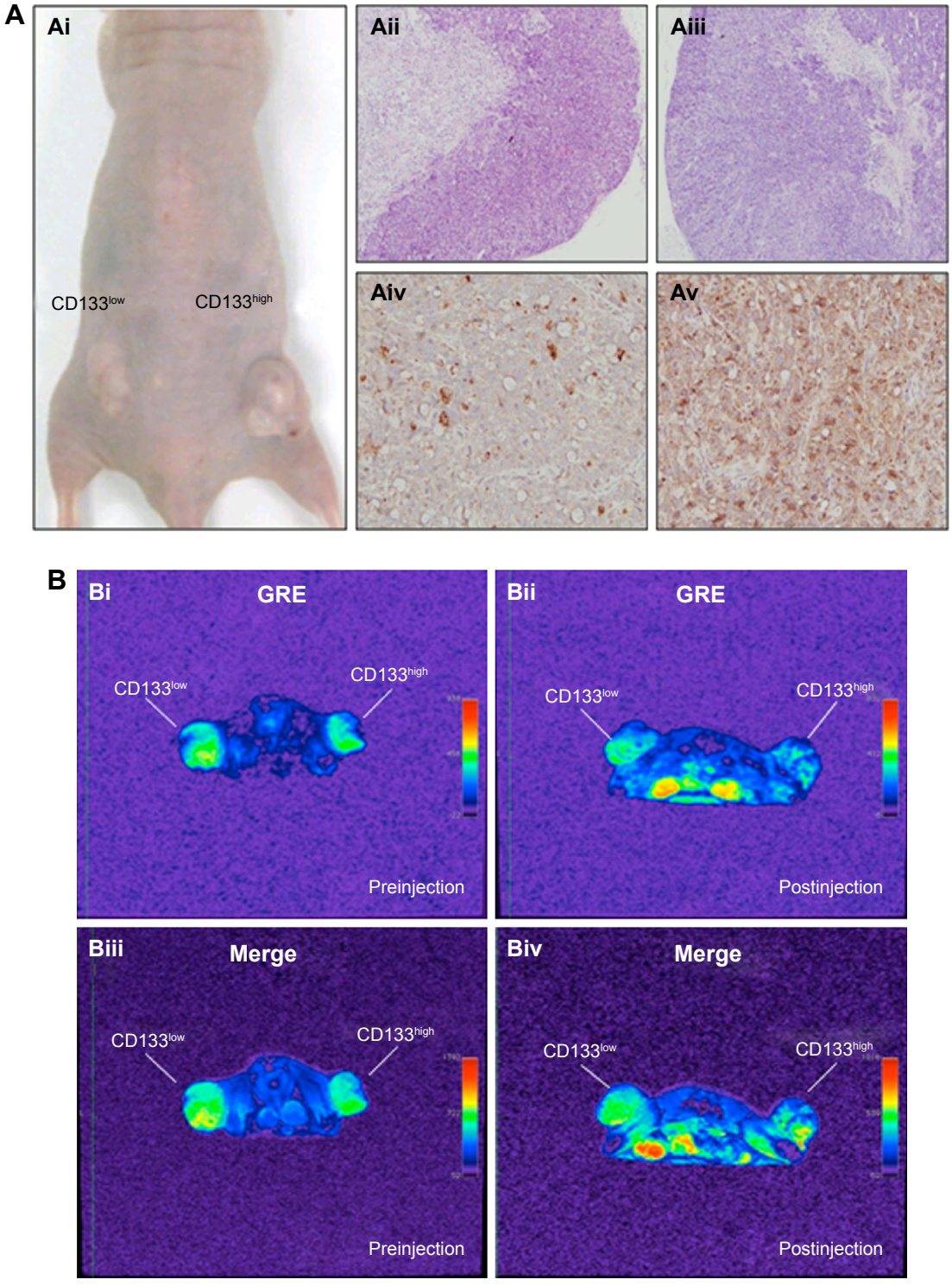

Figure 5 (*Continued*)

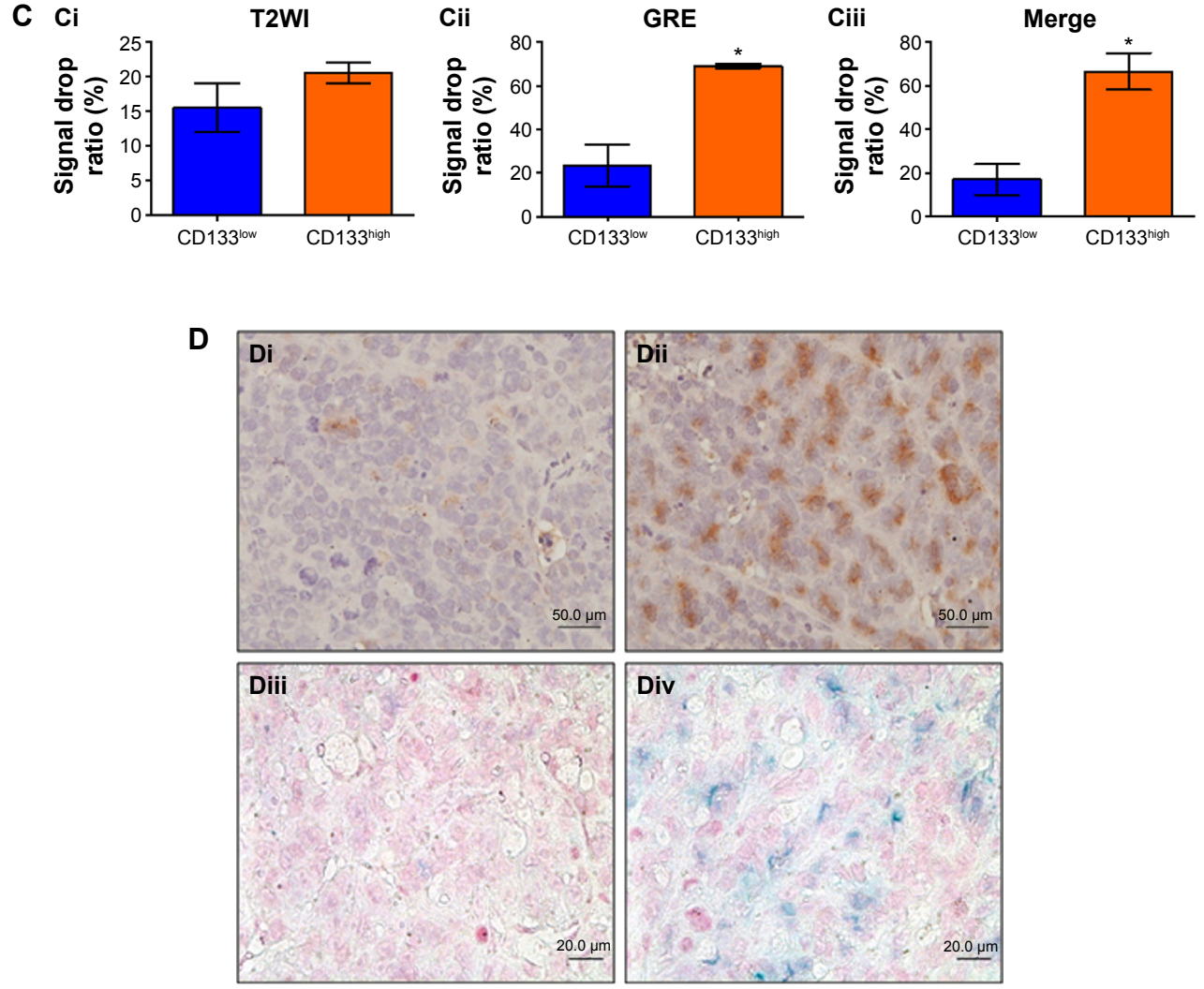

Figure 5 Detection of in vivo labeling by USPIO-CD133 Ab in CD133-positive subcutaneous xenografts by MRI.

Notes: (**A**) Photographs of CD133^{high} and CD133^{low} HT29 subcutaneous xenografts after subcutaneous inoculation of FACS-sorted CD133^{high} and CD133^{low} HT29 cells (**Ai**). H&E staining and differential CD133 immunostaining in CD133^{low} (**Aii** and **Aiv**) and CD133^{high} (**Aiii** and **Av**) xenografts at 400× magnification. (**B**) Gradient-echo (GRE) and multiple echo recombined gradient echo (Merge) images of CD133^{high} and CD133^{low} HT29 subcutaneous xenografts were acquired before (**Bi** and **Biii**, preinjection) and after (**Bii** and **Biv**, postinjection) intravenous injection of USPIO-CD133 Ab for 24 hours. (**C**) The representative signal drop ratio of MR images, including T2WI (**Ci**), multiecho GRE image (**Cii**), and Merge image (**Ciii**) after USPIO-CD133 Ab injection. Bar, SE; $^{*}P<0.05$. (**D**) CD133 immunohistochemical analysis showed that the CD133^{high} xenografts (**Di**) demonstrated stronger CD133 expression than the CD133^{low} xenografts (**Dii**) at 400× magnification. When compared to CD133^{low} xenografts (**Diii**), CD133^{high} xenografts (**Div**) accumulated more iron as seen by Prussian blue staining at 1,000× magnification.

Abbreviations: FACS, fluorescence-activated cell sorting; GRE, gradient-echo; H&E, hematoxylin and eosin; Merge, multiple echo recombined gradient echo; MRI, magnetic resonance imaging; SE, standard error of the mean; T2WI, T2 weighted image; USPIO-CD133 Ab, ultrasmall superparamagnetic iron oxide conjugated with anti-CD133 antibodies.

staining indicated that USPIO-CD133 Ab primarily targeted CD133-expressing cells and that USPIO-CD133 Ab was not taken up intracellularly by microglia. These data suggested that USPIO-CD133 Ab could be specifically and actively delivered to CD133-positive tumor cells in ENU-induced brain tumors (Figure 7B).

Discussion

One of the great challenges of oncology is to improve noninvasive methods for early tumor detection and for follow-up of tumor progression/regression during the course of therapy. Molecular imaging is defined as the characterization and measurement of biological processes at the cellular and molecular levels. Molecular imaging probes specifically target cancer markers that have been identified for disease-specific detection and personalized therapeutics.[47] Because of their unique magnetic features, conjugation of SPIO/USPIO nanoparticles with antibodies have been commercially used for a flexible, fast, and simple magnetic sorting system for in vitro separation of large numbers of cells according to specific cell-surface markers. Therefore, SPIO/USPIO nanoparticles conjugated with ligands specifically targeting tumors provide the possibility of MRI for precise molecular targets, and many significant advances have recently been seen in this

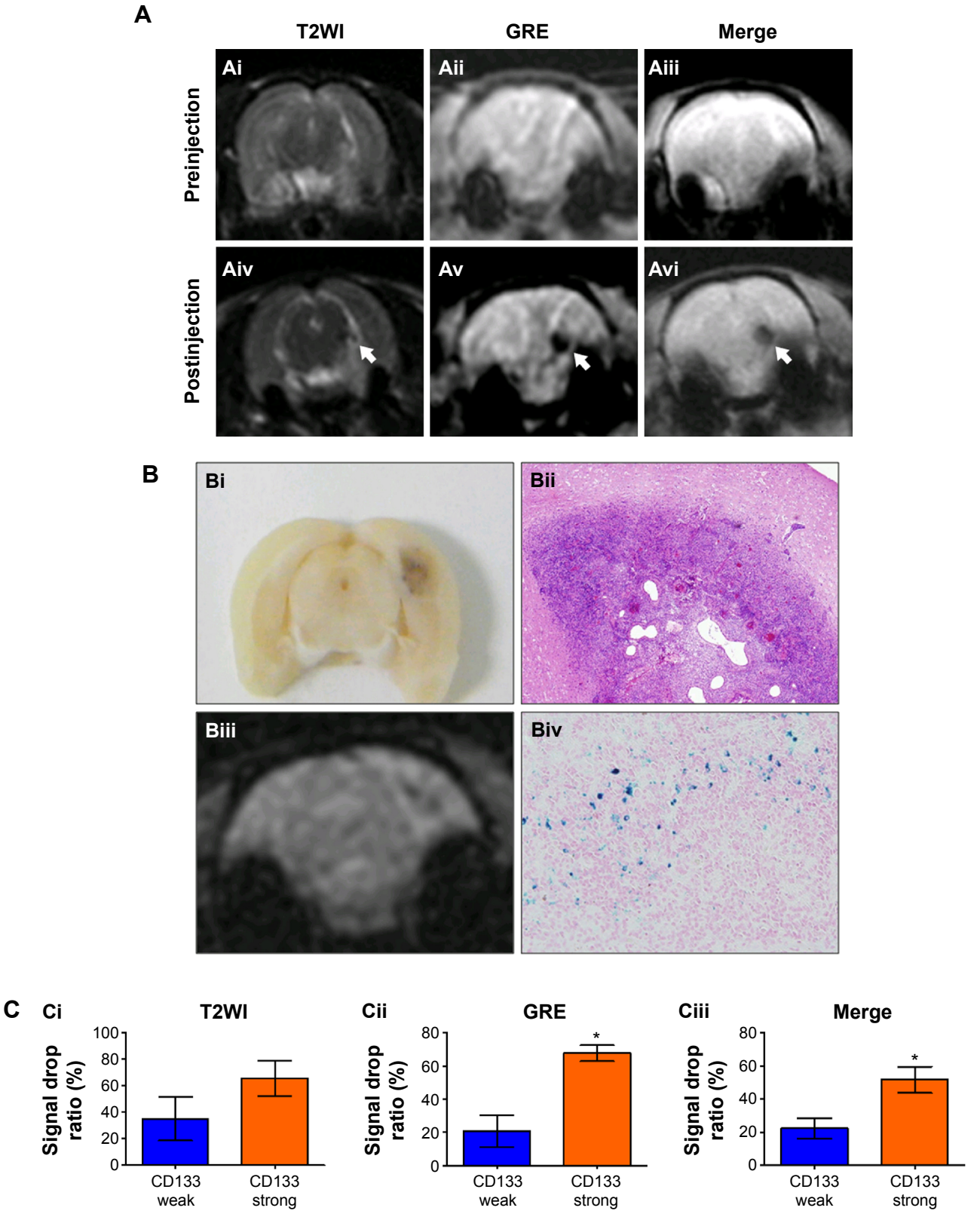

Figure 6 In vivo labeling of USPIO-CD133 Ab in ENU-induced rat brain tumors.

Notes: (**A**) Hypointensity of MRI signals after intravenous injection of USPIO-CD133 Ab. In T2 weighted images (**Ai** and **Aiv**), multiecho GRE images (**Aii** and **Av**), and Merge images (**Aiii** and **Avi**), MRI signals significantly decreased (white arrow) before (**Ai**–**Aiii**) and after (**Aiv**–**Av**) injection of USPIO-CD133 Ab for 24 hours. (**B**) USPIO-CD133 Ab decreased the signals of magnetic resonance (MR) imaging in ENU-induced rat brain tumors. (**Bi**) Gross view. (**Bii**) H&E staining at 100× magnification. (**Biii**) Multiple echo recombined gradient echo (Merge) image. (**Biv**) Prussian blue staining at 200× magnification in ENU-induced rat brain tumors. (**C**) The representative signal drop ratio of MR images, including T2WI (**Ci**), multiecho GRE images (**Cii**), and Merge images (**Ciii**) after USPIO-CD133 Ab injection. Bar, SE; $^{*}P<0.05$.

Abbreviations: ENU, *N*-ethyl-*N*-nitrosourea; H&E, hematoxylin and eosin; GRE, gradient-echo; Merge, multiple echo recombined gradient echo; SE, standard error of the mean; T2WI, T2 weighted image; USPIO-CD133 Ab, ultrasmall superparamagnetic iron oxide conjugated with anti-CD133 antibodies.

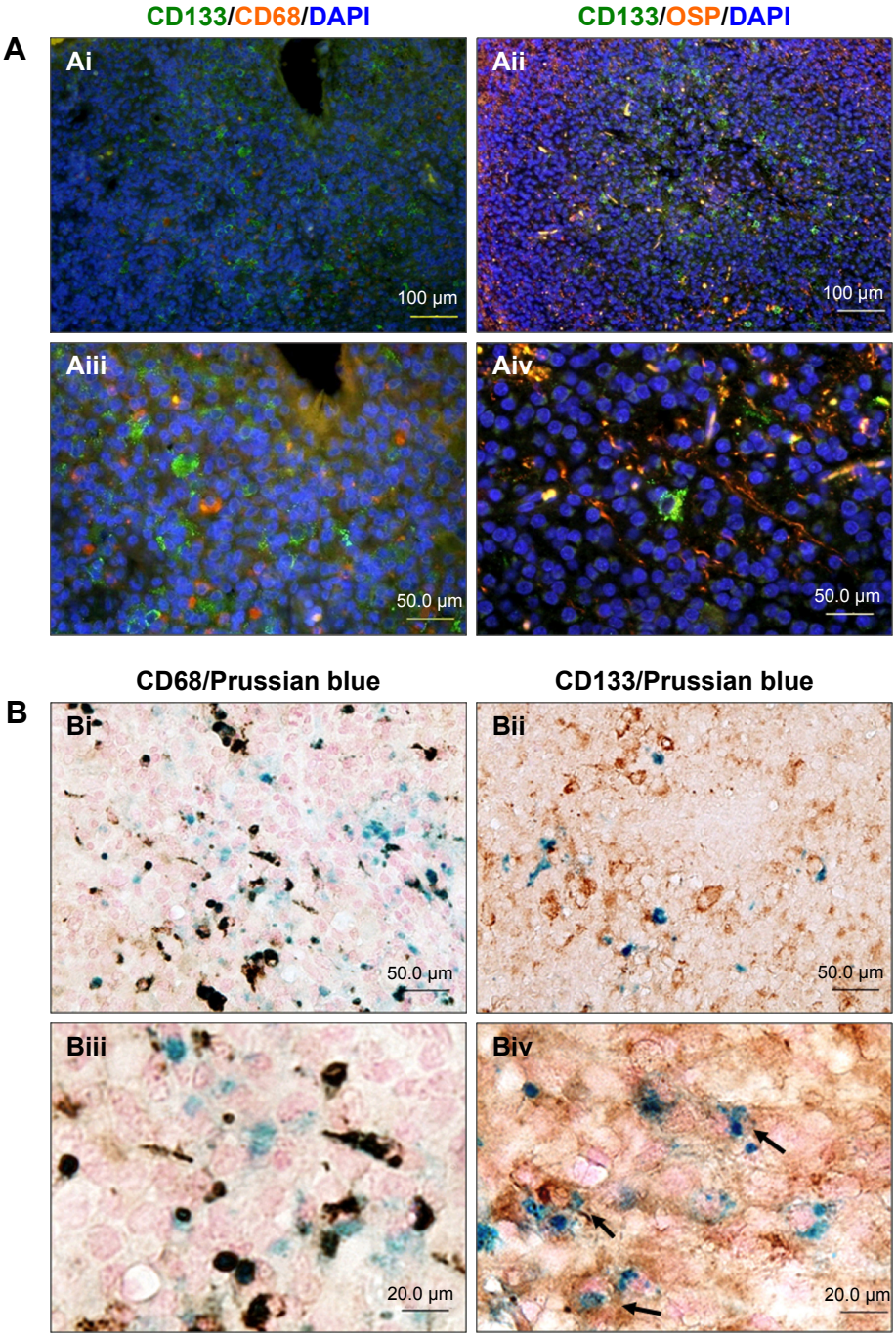

Figure 7 USPIO-CD133 Ab specifically targeted to ENU-induced rat brain tumor cells.
Notes: (**A**) Immunofluorescence staining of CD133 expression in microglia (CD68) and oligodendrocytes (oligodendrocyte-specific protein; [OSP]) of ENU-induced rat brain tumors was observed under fluorescent microscope at 200× (**Ai** and **Aii**) and 400× (**Aiii** and **Aiv**) magnification. (**B**) Detection of CD68 and CD133 expression in USPIO-CD133 Ab labeled cells of ENU-induced rat brain tumors. Double staining of CD133 (brown) and USPIO-CD133 Ab (Prussian blue staining) cells (indicated with arrows in **Biv**) are shown in the brain sections at 400× (**Bi** and **Bii**) and 1,000× (**Biii** and **Biv**) magnification.
Abbreviations: DAPI, 4′,6-diamidino-2-phenylindole; ENU, *N*-ethyl-*N*-nitrosourea; USPIO-CD133 Ab, ultrasmall superparamagnetic iron oxide conjugated with anti-CD133 antibodies.

field.[17,24,26–28,48–50] In this study, USPIO was conjugated with antibodies for the recognition of CD133, a surface marker associated with colorectal cancer and brain tumors, among other cancers, to produce a novel targeted contrast agent for detecting CSCs in vivo. Observed from transmission electron microscopy, the mean core diameter of whole particles was 29±7.9 nm, which assured efficient targeting and optical imaging of tumors in vitro and in vivo (Figure 1).[51]

Similar to the previous studies, the binding specificity of USPIO-CD133 Ab to CD133-expressing tumor cells was confirmed in vitro and in vivo by Prussian stain and MRI.[27,29,52–54] The in vitro study was designed to assess

the feasibility of clinical use of MR equipment at 1.5T to detect USPIO-CD133 Ab bound to tumor cells. The dose–response relationship was demonstrated between the amounts of USPIO-CD133 Ab bound to the cells on T2-weighted images as demonstrated previously (Figure 2B).[55–57] This effect is stronger in cells expressing high levels of CD133 ($CD133^{high}$ tumors) than in cells with lower levels of CD133 expression ($CD133^{low}$ tumors), indicating that the observed decrease in MR signaling depends both on the dose of the immunospecific contrast agent and on the target antigen expression levels of the tumor cells (Figure 5B and C). The changes in the in vivo MRI signal correlated with Prussian blue staining of tumor specimens. Sections from $CD133^{high}$ tumors but not $CD133^{low}$ tumors showed the presence of nanoparticles (Figure 5D). Indeed, in vivo experiments indicated that the intravenous administration of a single dose of USPIO-CD133 Ab, 18–24 hours before performing a 1.5T MRI scan, is sufficient to show a detectable change in signal. This decrease in MR signaling was detected in GRE and Merge images after injection of nanoparticles (Figures 5C and 6C). Similar to other studies for antibody-functionalized iron nanoparticles, our data suggested that the novel USPIO-CD133 Ab could differentially bind and have the potential to serve as a targeted contrast agent in CSC detection and monitoring by MRI (Figure 5).[24–27,53] Consistent with the study regarding to in vivo detection of c-Met expression in rat hepatocarcinogenesis model, intravenous injection of USPIO-CD133 Ab successfully targets and labels the tumor cells in rat tumor models.[58]

Studies have shown that polymer-coated nanoparticles, such as USPIO used in the present study, have no or minimal impact on cell viability, proliferation, ROS formation, apoptosis rate, and function, and that they have low toxicity in the majority of cells studied.[51,59,60] Similarly, any early toxic effects of USPIO-CD133 Ab were excluded on HT29 cells that might interfere with the phagocytosis of the particles. The MTS analysis demonstrated no effect on cell proliferation and viability with various concentrations of USPIO-CD133 Ab labeling of HT29, HepG2, and OC2 cells for 4 hours (Figures 3A and S3). Furthermore, a similarly low level of ROS was detected in HT29 cells with or without USPIO-CD133 Ab treatment (Figure 3C). Subsequent in vivo analysis of the USPIO-CD133 Ab showed the feasibility and safety of intravenous administration. The side effects, such as behavioral changes after the injection of particles in animals were not observed; however, the chronic toxicity of the magnetic nanoparticles was not analyzed due to their accumulation in the organs, such as livers (Figure S6). Several studies have clinically approved that SPIO MRI contrast agents such as Feridex and Resovist are safe and lack cytotoxicity.[61] Similar to other studies, our data demonstrated that USPIO-CD133 Ab displayed good biocompatibility and no significant cytotoxicity in tumor cells and in animals, suggesting that USPIO-CD133 can specifically and safely label CD133-positive cells in vitro and in vivo.[50,62]

The potential for intravenous nanoparticles targeting brain tumors has been actively debated, due to the blood–brain barrier and nonspecific uptake of particles by the endothelial system. However, it has been shown that the vascular structure in brain tumors is significantly different and is characterized by increased permeability.[63] A previous study reported that the detection of brain tumors with MRI and USPIO is based primarily on the visualization of labeled microglia and macrophages.[64] Targeted delivery may alter the intracellular distribution because the tumor cell internalization mechanism is enhanced by the presence of additional surface ligands.[65,66] Similar to other studies, our data demonstrated that oligodendrocytes but not microglial cells were actively recognized by USPIO-CD133 Ab, revealing the targeting selectivity of this agent (Figure 7).[26,50]

Similar to previous studies, a potential limitation of the present study may be the relatively low iron concentration in the USPIO-antibody conjugate in comparison with the clinically available nontargeted MRI contrast agents, which are nonspecifically trapped by reticulum-endothelial cells or taken up nonspecifically by macrophages within 24 hours of systemic administration.[67,68] Thus, the development of similar USPIO-targeted antibodies with a high iron-oxide content may allow enhanced sensitivity in detection to permit the MRI of tumors with small diameters or with lower target antigen densities. Additionally, Chertok et al reported that intracarotid administration demonstrated a 30-fold increase in tumor entrapment of nanoparticles compared to that seen with intravenous administration.[69] This result suggests that an increase in the intratumoral accumulation of nanoparticles may be achieved via different routes of administration. Although the efficiency of mAb-targeted USPIO has been demonstrated in several studies, the big-size antibodies limit the abilities of antibody-conjugated nanoparticles permeate through the vasculature into the tumor areas.[26,27,29] In addition, the interaction of antibody with Fc receptors on normal tissues can change the specificity of tumor-targeted nanoparticles. To solve these problems, CD133-binding peptides or single-chain antibodies with small molecular weight can be used as targets for engineering targeted nanoparticles.[70] Furthermore, using

species-specific antibodies may reduce immunogenicity usually described when murine antibodies were injected in different species or humans.[71]

Recently, modification of the magnetic nanoparticles by various agents, such as chemotherapy drugs, has indicated their therapeutic potency.[72] It is likely that the conjugation of USPIO-CD133 Ab with anticancer drugs could increase the specificity of targeted drug delivery and reduce the side effects of these drugs. Additionally, optimizing new generations of USPIO-antibodies or other USPIO-ligands that are able to specifically bind and sensitively detect tumor-associated markers may provide valuable immunospecific contrast agents for the diagnosis of tumors and the targeting of cancer therapies. This study demonstrated that mAb nanodevices are useful for specifically targeting tumors by clinical 1.5T MRI and that a stable conformation of nanoparticles with targeting ability in vivo is achievable, given that the USPIO-mAb accumulated gradually in CD133-positive tumors. The future development of background-free nanoparticles and detection systems will contribute to the use of such mAb nanodevices for tumor-specific MRI diagnosis.

Conclusion

CD133-associated mAbs coupled with USPIO nanoparticles can be taken up in a specific manner by CD133-expressing tumor cells, and specifically shorten the T2 values of CD133-expressing xenografts in an MRI scanner. In ENU-induced rat brain tumors, several clusters of hypointensive zones were observed by MRI after intravenously administered USPIO-CD133 Ab. The USPIO-CD133 Ab specifically recognizes and labels the CD133 molecule in CD133-expressing tumor cells in vivo, as validated using IHC with anti-CD133 antibodies and Prussian blue staining for iron levels. Therefore, this nanoparticle probe can be used as an MRI-specific contrast agent for detecting and extracellularly tracking CD133-positive tumor cells in vitro and in vivo.

Acknowledgments

This study was supported by grants NSC 99-2314-B-006-018-MY3, MOST 103-2314-B-400-010, and MOHW103-TDU-212-114005 from the National Science Council, Ministry of Science and Technology, and Department of Health, Taiwan. The authors thank the Institute of Molecular Biology, Academia Sinica, for kindly providing an FEI Tecnai G2 spirit EM, and Dr Chung-Shi Yang at the Institute of Biomedical Engineering and Nanomedicine, National Health Research Institutes, for kindly providing a Hitachi H7650 EM. The authors thank Dr Shieh-Yueh Yang, MagQu Co. Ltd, Taiwan, for providing the information of functionalized-antibody nanoparticles in the revision of manuscript.

Disclosure

The authors report no conflicts of interest in this work.

References

1. Michor F, Hughes TP, Iwasa Y, et al. Dynamics of chronic myeloid leukaemia. *Nature*. 2005;435(7046):1267–1270.
2. Huntly BJ, Gilliland DG. Cancer biology: summing up cancer stem cells. *Nature*. 2005;435(7046):1169–1170.
3. Pfenninger CV, Roschupkina T, Hertwig F, et al. CD133 is not present on neurogenic astrocytes in the adult subventricular zone, but on embryonic neural stem cells, ependymal cells, and glioblastoma cells. *Cancer Res*. 2007;67(12):5727–5736.
4. Yi JM, Tsai HC, Glockner SC, et al. Abnormal DNA methylation of CD133 in colorectal and glioblastoma tumors. *Cancer Res*. 2008;68(19):8094–8103.
5. Miraglia S, Godfrey W, Yin AH, et al. A novel five-transmembrane hematopoietic stem cell antigen: isolation, characterization, and molecular cloning. *Blood*. 1997;90(12):5013–5021.
6. Bhatia M. AC133 expression in human stem cells. *Leukemia*. 2001;15(11):1685–1688.
7. Corbeil D, Roper K, Hellwig A, et al. The human AC133 hematopoietic stem cell antigen is also expressed in epithelial cells and targeted to plasma membrane protrusions. *J Biol Chem*. 2000;275(8):5512–5520.
8. Rafii S. Circulating endothelial precursors: mystery, reality, and promise. *J Clin Invest*. 2000;105(1):17–19.
9. Singh SK, Clarke ID, Terasaki M, et al. Identification of a cancer stem cell in human brain tumors. *Cancer Res*. 2003;63(18):5821–5828.
10. Singh SK, Hawkins C, Clarke ID, et al. Identification of human brain tumour initiating cells. *Nature*. 2004;432(7015):396–401.
11. Yin S, Li J, Hu C, et al. CD133 positive hepatocellular carcinoma cells possess high capacity for tumorigenicity. *Int J Cancer*. 2007;120(7):1444–1450.
12. Yang K, Chen XZ, Zhang B, et al. Is CD133 a biomarker for cancer stem cells of colorectal cancer and brain tumors? A meta-analysis. *Int J Biol Markers*. 2011;26(3):173–180.
13. Xia P. Surface markers of cancer stem cells in solid tumors. *Curr Stem Cell Res Ther*. 2013;9(2):102–111.
14. Moghbeli M, Moghbeli F, Forghanifard MM, Abbaszadegan MR. Cancer stem cell detection and isolation. *Med Oncol*. 2014;31(9):69.
15. Maitland NJ, Collins AT. Cancer stem cells – a therapeutic target? *Curr Opin Mol Ther*. 2010;12(6):662–673.
16. Allegra A, Alonci A, Penna G, et al. The cancer stem cell hypothesis: a guide to potential molecular targets. *Cancer Invest*. 2014;32(9):470–495.
17. Islam T, Josephson L. Current state and future applications of active targeting in malignancies using superparamagnetic iron oxide nanoparticles. *Cancer Biomark*. 2009;5(2):99–107.
18. Weissleder R, Elizondo G, Wittenberg J, Rabito CA, Bengele HH, Josephson L. Ultrasmall superparamagnetic iron oxide: characterization of a new class of contrast agents for MR imaging. *Radiology*. 1990;175(2):489–493.
19. Tanimoto A, Oshio K, Suematsu M, Pouliquen D, Stark DD. Relaxation effects of clustered particles. *J Magn Reson Imaging*. 2001;14(1):72–77.
20. Gossuin Y, Gillis P, Hocq A, Vuong QL, Roch A. Magnetic resonance relaxation properties of superparamagnetic particles. *Wiley Interdiscip Rev Nanomed Nanobiotechnol*. 2009;1(3):299–310.
21. Himmelreich U, Dresselaers T. Cell labeling and tracking for experimental models using magnetic resonance imaging. *Methods*. 2009;48(2):112–124.
22. Corot C, Robert P, Idee JM, Port M. Recent advances in iron oxide nanocrystal technology for medical imaging. *Adv Drug Deliv Rev*. 2006;58(14):1471–1504.

23. Zhang C, Jugold M, Woenne EC, et al. Specific targeting of tumor angiogenesis by RGD-conjugated ultrasmall superparamagnetic iron oxide particles using a clinical 1.5-T magnetic resonance scanner. *Cancer Res*. 2007;67(4):1555–1562.
24. Baio G, Fabbi M, de Totero D, et al. Magnetic resonance imaging at 1.5T with immunospecific contrast agent in vitro and in vivo in a xenotransplant model. *MAGMA*. 2006;19(6):313–320.
25. Baio G, Fabbi M, Salvi S, et al. Two-step in vivo tumor targeting by biotin-conjugated antibodies and superparamagnetic nanoparticles assessed by magnetic resonance imaging at 1.5 T. *Mol Imaging Biol*. 2009; 12(3):305–315.
26. Huang KW, Chieh JJ, Lin IT, Horng HE, Yang HC, Hong CY. Anti-CEA-functionalized superparamagnetic iron oxide nanoparticles for examining colorectal tumors in vivo. *Nanoscale Res Lett*. 2013;8(1):413.
27. Hsieh WJ, Liang CJ, Chieh JJ, et al. In vivo tumor targeting and imaging with anti-vascular endothelial growth factor antibody-conjugated dextran-coated iron oxide nanoparticles. *Int J Nanomedicine*. 2012;7: 2833–2842.
28. Yang L, Peng XH, Wang YA, et al. Receptor-targeted nanoparticles for in vivo imaging of breast cancer. *Clin Cancer Res*. 2009;15(14): 4722–4732.
29. Shamsipour F, Zarnani AH, Ghods R, et al. Conjugation of monoclonal antibodies to super paramagnetic iron oxide nanoparticles for detection of her2/neu antigen on breast cancer cell lines. *Avicenna J Med Biotechnol*. 2009;1(1):27–31.
30. Wang X, Wei F, Liu A, et al. Cancer stem cell labeling using poly(L-lysine)-modified iron oxide nanoparticles. *Biomaterials*. 2012;33(14):3719–3732.
31. Wong DY, Chang KW, Chen CF, Chang RC. Characterization of two new cell lines derived from oral cavity human squamous cell carcinomas–OC1 and OC2. *J Oral Maxillofac Surg*. 1990;48(4):385–390.
32. Jiang W, Yang HC, Yang SY, et al. Preparation and properties of superparamagnetic nanoparticles with narrow size distribution and biocompatible. *J Magn Magn Mater*. 2004;283(2–3):210–214.
33. Horng HE, Yang SY, Huang YW, Jiang WQ, Hong CY, Yang HC. Nanomagnetic particles for SQUID-based magnetically labeled immunoassay. *IEEE Trans Appl Supercond*. 2005;15(2):668–671.
34. Yang SY, Jian ZF, Horng HE, et al. Dual immobilization and magnetic manipulation of magnetic nanoparticles. *J Magn Magn Mater*. 2008;320(21):2688–2691.
35. Huang KW, Yang SY, Horng HE, et al. Time-evolution contrast of target MRI using high-stability antibody functionalized magnetic nanoparticles: an animal model. *J Nanomater*. 2014;2014:351848.
36. Hong C-Y, Chen WS, Jian ZF, et al. Wash-free immunomagnetic detection for serum through magnetic susceptibility reduction. *Appl Phys Lett*. 2007;90(7):074105.
37. Yang CC, Huang KW, Yang SY, et al. Development for high-accuracy in vitro assay of vascular endothelial growth factor using nanomagnetically labeled immunoassay. *J Nanomater*. 2013;2013:695276.
38. Yang CC, Yang SY, Ho CS, Chang JF, Liu BH, Huang KW. Development of antibody functionalized magnetic nanoparticles for the immunoassay of carcinoembryonic antigen: a feasibility study for clinical use. *J Nanobiotechnol*. 2014;12(1):44.
39. Chen FJ, Lee KW, Lai CC, et al. Structure of native oligomeric Sprouty2 by electron microscopy and its property of electroconductivity. *Biochem Biophys Res Commun*. 2013;439(3):351–356.
40. Pawelczyk E, Arbab AS, Pandit S, Hu E, Frank JA. Expression of transferrin receptor and ferritin following ferumoxides-protamine sulfate labeling of cells: implications for cellular magnetic resonance imaging. *NMR Biomed*. 2006;19(5):581–592.
41. Chen YW, Tsai MY, Pan HB, Tseng HH, Hung YT, Chou CP. Gadoxetic acid-enhanced MRI and sonoelastography: non-invasive assessments of chemoprevention of liver fibrosis in thioacetamide-induced rats with sho-saiko-to. *PLoS One*. 2014;9(12):e114756.
42. Stahn R, Rose S, Sanborn S, West G, Herschman H. Effects of nerve growth factor administration of N-ethyl-N-nitrosourea carcinogenesis. *Brain Res*. 1975;96(2):287–298.
43. Habs M, Schmahl D. Influence of five different postnatal lifelong treatments on the transplacental carcinogenicity of ethylnitrosourea in Sprague-Dawley rats. *Cancer Lett*. 1976;2(2):93–100.
44. Ieta K, Tanaka F, Haraguchi N, et al. Biological and genetic characteristics of tumor-initiating cells in colon cancer. *Ann Surg Oncol*. 2008;15(2):638–648.
45. Sharifi S, Behzadi S, Laurent S, Forrest ML, Stroeve P, Mahmoudi M. Toxicity of nanomaterials. *Chem Soc Rev*. 2012;41(6):2323–2343.
46. Kim JE, Shin JY, Cho MH. Magnetic nanoparticles: an update of application for drug delivery and possible toxic effects. *Arch Toxicol*. 2012;86(5):685–700.
47. Rosenblum LT, Kosaka N, Mitsunaga M, Choyke PL, Kobayashi H. In vivo molecular imaging using nanomaterials: general in vivo characteristics of nano-sized reagents and applications for cancer diagnosis. *Mol Membr Biol*. 2010;27(7):274–285.
48. Peng XH, Qian X, Mao H, et al. Targeted magnetic iron oxide nanoparticles for tumor imaging and therapy. *Int J Nanomedicine*. 2008;3(3): 311–321.
49. Jiang T, Zhang C, Zheng X, et al. Noninvasively characterizing the different alphavbeta3 expression patterns in lung cancers with RGD-USPIO using a clinical 3.0T MR scanner. *Int J Nanomedicine*. 2009;4: 241–249.
50. Shevtsov MA, Nikolaev BP, Yakovleva LY, et al. Superparamagnetic iron oxide nanoparticles conjugated with epidermal growth factor (SPION-EGF) for targeting brain tumors. *Int J Nanomedicine*. 2014;9: 273–287.
51. Sun R, Dittrich J, Le-Huu M, et al. Physical and biological characterization of superparamagnetic iron oxide- and ultrasmall superparamagnetic iron oxide-labeled cells: a comparison. *Invest Radiol*. 2005; 40(8):504–513.
52. Guo Q, Liu Y, Xu K, Ren K, Sun W. Mouse lymphatic endothelial cell targeted probes: anti-LYVE-1 antibody-based magnetic nanoparticles. *Int J Nanomedicine*. 2013;8:2273–2284.
53. Chen H, Wang L, Yu Q, et al. Anti-HER2 antibody and ScFvEGFR-conjugated antifouling magnetic iron oxide nanoparticles for targeting and magnetic resonance imaging of breast cancer. *Int J Nanomedicine*. 2013;8:3781–3794.
54. Wang X, Xing X, Zhang B, Liu F, Cheng Y, Shi D. Surface engineered antifouling optomagnetic SPIONs for bimodal targeted imaging of pancreatic cancer cells. *Int J Nanomedicine*. 2014;9:1601–1615.
55. Moore A, Medarova Z, Potthast A, Dai G. In vivo targeting of underglycosylated MUC-1 tumor antigen using a multimodal imaging probe. *Cancer Res*. 2004;64(5):1821–1827.
56. Simberg D, Duza T, Park JH, et al. Biomimetic amplification of nanoparticle homing to tumors. *Proc Natl Acad Sci U S A*. 2007;104(3): 932–936.
57. Al Faraj A, Shaik AS, Afzal S, Al Sayed B, Halwani R. MR imaging and targeting of a specific alveolar macrophage subpopulation in LPS-induced COPD animal model using antibody-conjugated magnetic nanoparticles. *Int J Nanomedicine*. 2014;9:1491–1503.
58. Towner RA, Smith N, Tesiram YA, et al. In vivo detection of c-MET expression in a rat hepatocarcinogenesis model using molecularly targeted magnetic resonance imaging. *Mol Imaging*. 2007;6(1):18–29.
59. Thorek DL, Chen AK, Czupryna J, Tsourkas A. Superparamagnetic iron oxide nanoparticle probes for molecular imaging. *Ann Biomed Eng*. 2006;34(1):23–38.
60. Arbab AS, Yocum GT, Rad AM, et al. Labeling of cells with ferumoxides-protamine sulfate complexes does not inhibit function or differentiation capacity of hematopoietic or mesenchymal stem cells. *NMR Biomed*. 2005;18(8):553–559.
61. Wang YX. Superparamagnetic iron oxide based MRI contrast agents: current status of clinical application. *Quant Imaging Med Surg*. 2012; 1(1):35–40.
62. Schlachter EK, Widmer HR, Bregy A, et al. Metabolic pathway and distribution of superparamagnetic iron oxide nanoparticles: in vivo study. *Int J Nanomedicine*. 2011;6:1793–1800.

63. Chertok B, David AE, Yang VC. Brain tumor targeting of magnetic nanoparticles for potential drug delivery: effect of administration route and magnetic field topography. *J Control Release*. 2011;155(3):393–399.
64. Fleige G, Nolte C, Synowitz M, Seeberger F, Kettenmann H, Zimmer C. Magnetic labeling of activated microglia in experimental gliomas. *Neoplasia*. 2001;3(6):489–499.
65. Prokop A, Davidson JM. Nanovehicular intracellular delivery systems. *J Pharm Sci*. 2008;97(9):3518–3590.
66. Wang M, Thanou M. Targeting nanoparticles to cancer. *Pharmacol Res*. 2010;62(2):90–99.
67. Wang YX, Hussain SM, Krestin GP. Superparamagnetic iron oxide contrast agents: physicochemical characteristics and applications in MR imaging. *Eur Radiol*. 2001;11(11):2319–2331.
68. Huang X, Peng X, Wang Y, Shin DM, El-Sayed MA, Nie S. A reexamination of active and passive tumor targeting by using rod-shaped gold nanocrystals and covalently conjugated peptide ligands. *ACS Nano*. 2010;4(10):5887–5896.
69. Chertok B, Moffat BA, David AE, et al. Iron oxide nanoparticles as a drug delivery vehicle for MRI monitored magnetic targeting of brain tumors. *Biomaterials*. 2008;29(4):487–496.
70. Sun J, Zhang C, Liu G, et al. A novel mouse CD133 binding-peptide screened by phage display inhibits cancer cell motility in vitro. *Clin Exp Metastasis*. 2012;29(3):185–196.
71. Gonzales NR, De Pascalis R, Schlom J, Kashmiri SV. Minimizing the immunogenicity of antibodies for clinical application. *Tumour Biol*. 2005;26(1):31–43.
72. Jalalian SH, Taghdisi SM, Shahidi Hamedani N, et al. Epirubicin loaded super paramagnetic iron oxide nanoparticle-aptamer bioconjugate for combined colon cancer therapy and imaging in vivo. *Eur J Pharm Sci*. 2013;50(2):191–197.

Supplementary materials

Western blot

Cell lysate was obtained by harvesting cells in radioimmunoprecipitation assay buffer containing 50 mM Tris-HCl (pH 8.0), 150 mM NaCl (Sigma-Aldrich, St Louis, MO, USA), 0.5% sodium deoxycholate (Sigma-Aldrich), 1% NP-40 (Sigma-Aldrich), 0.1% sodium dodecyl sulfate (Sigma-Aldrich), and protease inhibitors (Complete, Roche, Basel, Switzerland). After centrifugation, cell extract was separated in sodium dodecyl sulfate polyacrylamide gel electrophoresis (sodium dodecyl sulfate-PAGE) and transferred onto polyvinyl difluoride (Bio-Rad Laboratories Inc., Hercules, CA, USA) membranes. Blots were probed with primary antibodies overnight at 4°C and then with secondary antibodies coupled with horseradish peroxidase for 1 hour at room temperature. Immunoreactivity was detected by chemiluminescence using Super Signal substrate (Pierce, Rockford, IL, USA) according to the manufacturer's protocols. The following antibodies were used in this study: CD133 (ab19898, Abcam, Cambridge, UK) and anti-β-actin (Cell Signaling, Beverly, MA, USA).

Flow cytometry and isolation of CD133-positive cells

Cultured cells were trypsinized and suspended in PBS. The CD133-positive cells were characterized by flow cytometry using mouse anti-human CD133/1-PE (Miltenyi Biotec, Bergisch Gladbach, Germany) monoclonal antibody. During staining, the cells were incubated at 4°C in the dark for 45 minutes. After incubation, the cells were washed and analyzed by a flow cytometer (FACS Calibur, BD Biosciences, San Jose, CA, USA). A minimum of 10,000 events was collected and acquired using CellQuest software (BD Biosciences). For $CD133^{high}$ cells sorting, cells were stained with CD133/1-PE and isolated on FACSAria Instruments (BD Biosciences). Positive and negative gates were determined using IgG-stained and unstained controls. Isolated cells were then washed twice with PBS and plated under the same conditions as unsorted cells. And then, we used CD133/2-PE (Miltenyi Biotec), an alternative antibody recognizing the second epitope of CD133 (CD133/2), to evaluate the sorting efficiency in the fluorescence-activated cell sorting experiment.

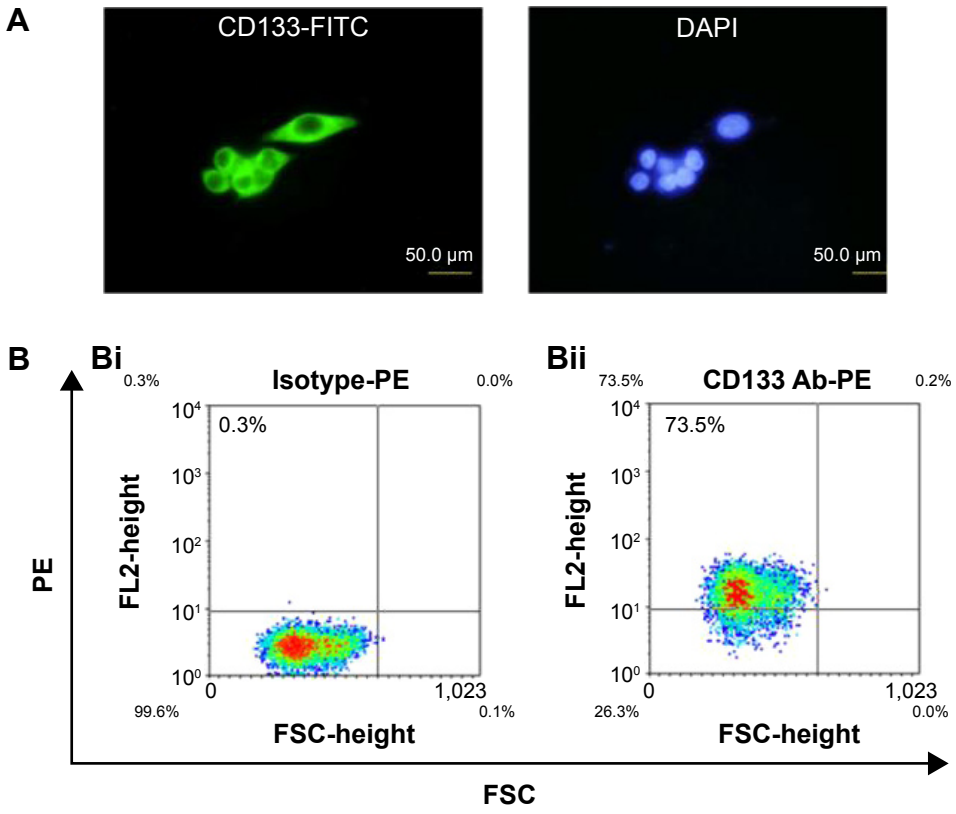

Figure S1 A high percentage of CD133-positive cells in HT29 cells.

Notes: (**A**) HT29 cells were stained with anti-CD133 antibody (green) and DAPI (blue) and observed under fluorescent microscope at 400× magnifications. (**B**) The percentage of CD133-positive HT29 cells was determined using flow cytometry. Using anti-CD133 Ab, the percentage of CD133-positive HT29 cells was analyzed from density plots (**Bii**). Isotype control antibodies served as a negative control (**Bi**).

Abbreviations: DAPI, 4′,6-diamidino-2-phenylindole; FITC, fluorescein isothiocyanate; FL, fluorescence; FSC, forward scatter; PE, phycoerythrin.

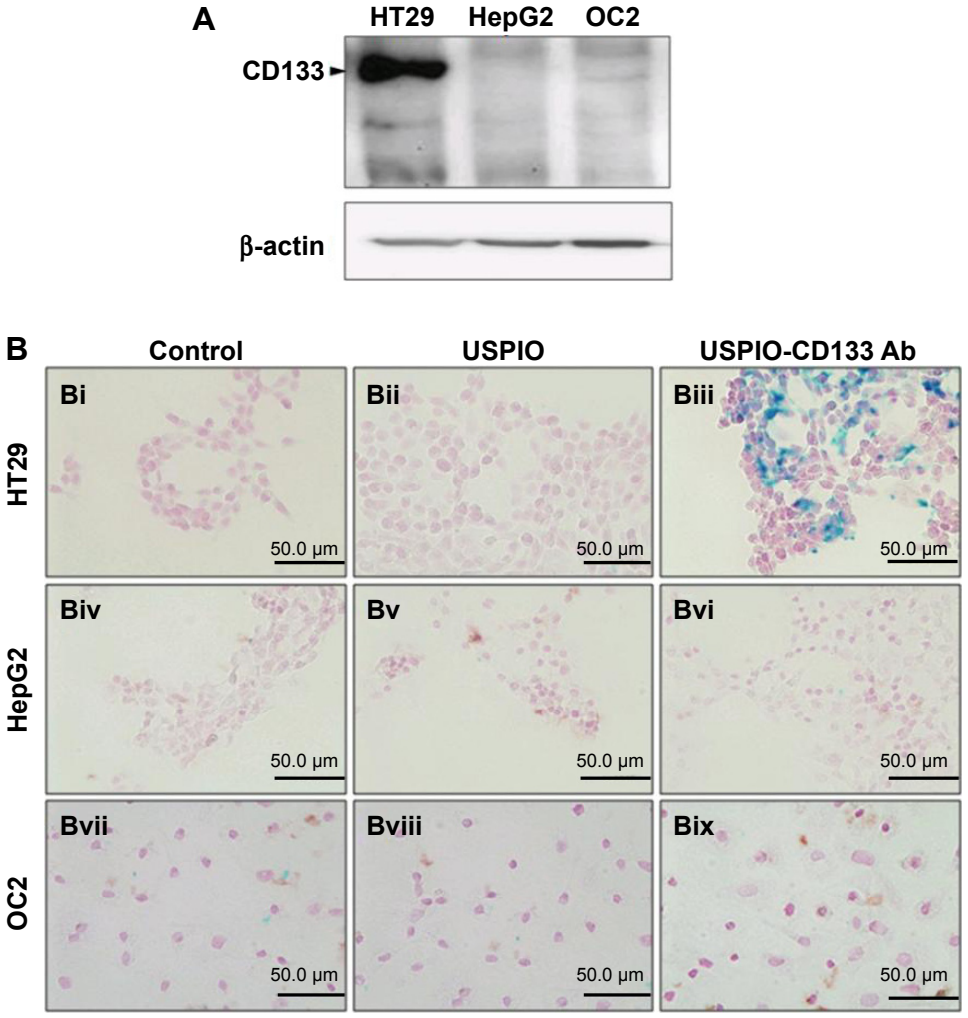

Figure S2 In vitro detection of USPIO-CD133 Ab binding to tumor cells using Prussian blue staining.
Notes: (**A**) Detection of CD133 expression in HT29, HepG2, and OC2 cells by Western blot. β-actin served as an internal control. (**B**) HT29, HepG2, and OC2 cells were incubated with PBS (**Bi**, **Biv**, and **Bvii**), USPIO (**Bii**, **Bv**, and **Bviii**), and USPIO-CD133 Ab (**Biii**, **Bvi**, and **Bix**), and the iron location detected by Prussian blue staining at 400× magnification.
Abbreviations: PBS, phosphate-buffered saline; USPIO, ultrasmall superparamagnetic iron oxide; USPIO-CD133 Ab, USPIO conjugated with anti-CD133 antibodies.

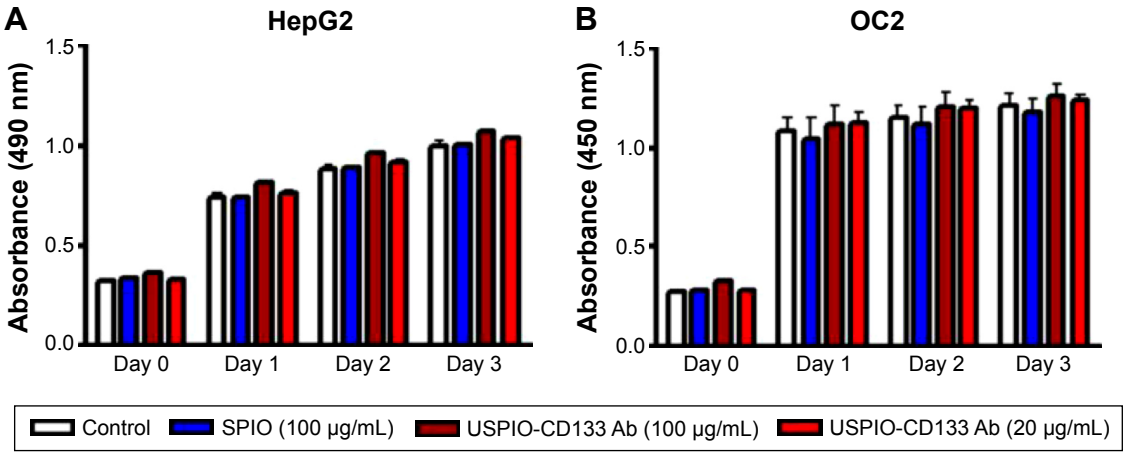

Figure S3 Effects of USPIO-CD133 Ab on cell growth of HepG2 and OC2 cells.
Notes: (**A**) No significant difference in cell growth was found between USPIO-CD133 Ab-labeled and unlabeled HepG2 analyzed by MTS assay. (**B**) No significant difference in cell growth was detected between USPIO-CD133 Ab-labeled and unlabeled OC2 cells analyzed by MTS assay.
Abbreviations: MTS, 3-(4,5-dimethylthiazol-2-yl)-5-(3-carboxymethoxyphenyl)-2-(4-sulfophenyl)-2H-tetrazolium; SPIO, superparamagnetic iron oxide; USPIO-CD133 Ab, ultrasmall SPIO conjugated with anti-CD133 antibodies.

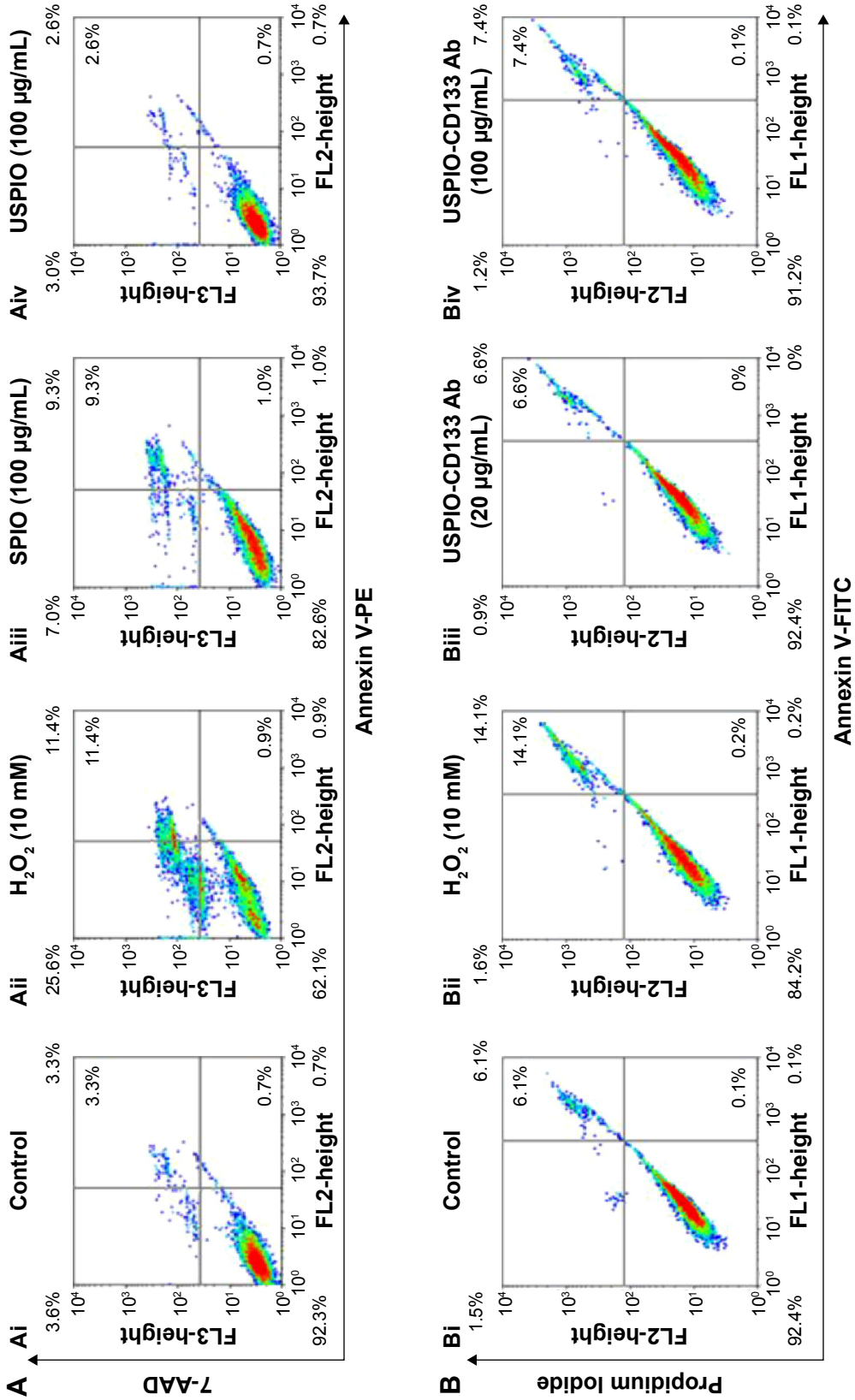

Figure S4 Cell apoptosis analysis of HT29 cells with different treatments by flow cytometry.

Notes: (**A**) Apoptosis analysis by detecting with Annexin V (FL2)/7-AAD (FL3) in HT29 cells without treatment (**Ai**); treated with H_2O_2 (**Aii**); labeled with 100 μg/mL of SPIO (**Aiii**); labeled with 100 μg/mL of USPIO (**Aiv**). (**B**) Apoptosis analysis by detecting with Annexin V (FL1)/PI (FL2) in HT29 cells without treatment (**Bi**); treated with H_2O_2 (**Bii**); labeled with 20 μg/mL of USPIO-CD133 Ab (**Biii**); labeled with 100 μg/mL of USPIO-CD133 Ab (**Biv**).

Abbreviations: 7-AAD, 7-aminoactinomycin D; FITC, fluorescein isothiocyanate; FL, fluorescence; PE, phycoerythrin; PI, propidium iodide; SPIO, superparamagnetic iron oxide; USPIO, ultrasmall SPIO; USPIO-CD133 Ab, USPIO conjugated with anti-CD133 antibodies.

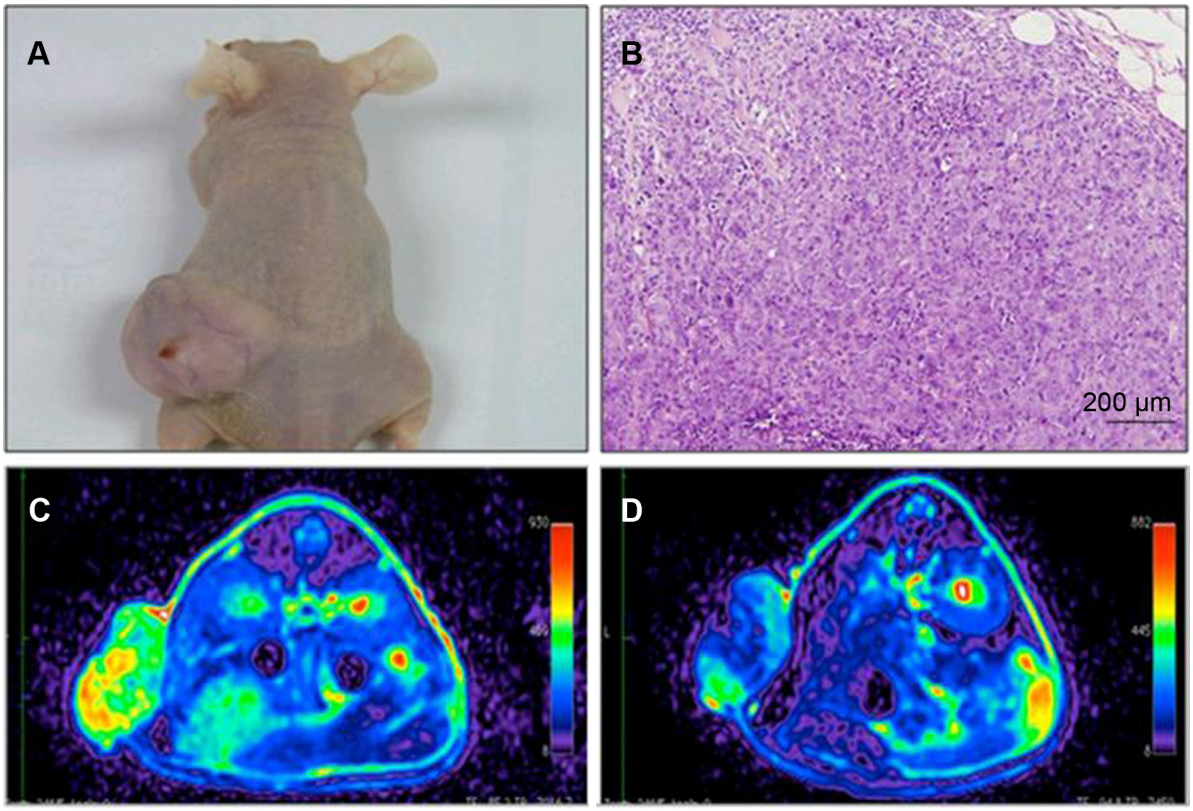

Figure S5 In vivo MR images of HT29 subcutaneous xenografts after intravenous injection of USPIO-CD133 Ab.
Notes: Photograph of tumor-bearing mouse (**A**); H&E staining of xenografted tumor at 100× magnification (**B**); FSE T2-weighted MR images of preinjection (**C**) and postinjection of USPIO-CD133 Ab for 24 hours (**D**).
Abbreviations: FSE, fast spin echo; H&E, hematoxylin and eosin; MR, magnetic resonance; USPIO, ultrasmall SPIO; USPIO-CD133 Ab, USPIO conjugated with anti-CD133 antibodies.

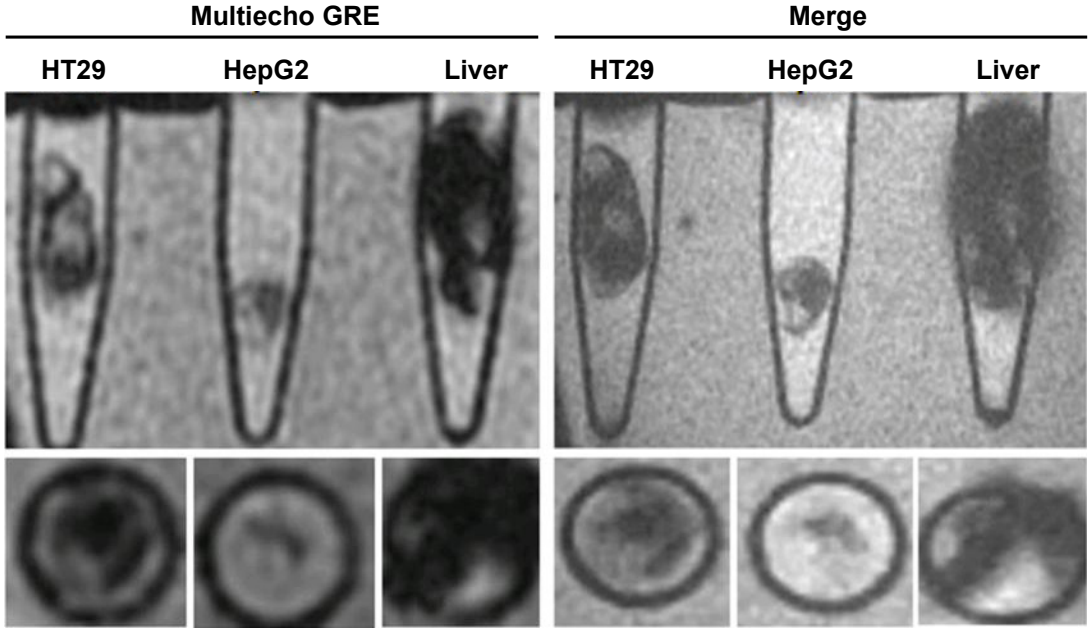

Figure S6 Gradient-echo (GRE) and multiple echo recombined gradient echo (Merge) images of HT29 and HepG2 subcutaneous xenografts were acquired after intravenous injection of USPIO-CD133 Ab for 48 hours. Liver tissues served as a reference for a positive control organ with marked signal drop.
Abbreviation: USPIO-CD133 Ab, ultrasmall superparamagnetic iron oxide conjugated with anti-CD133 antibodies.

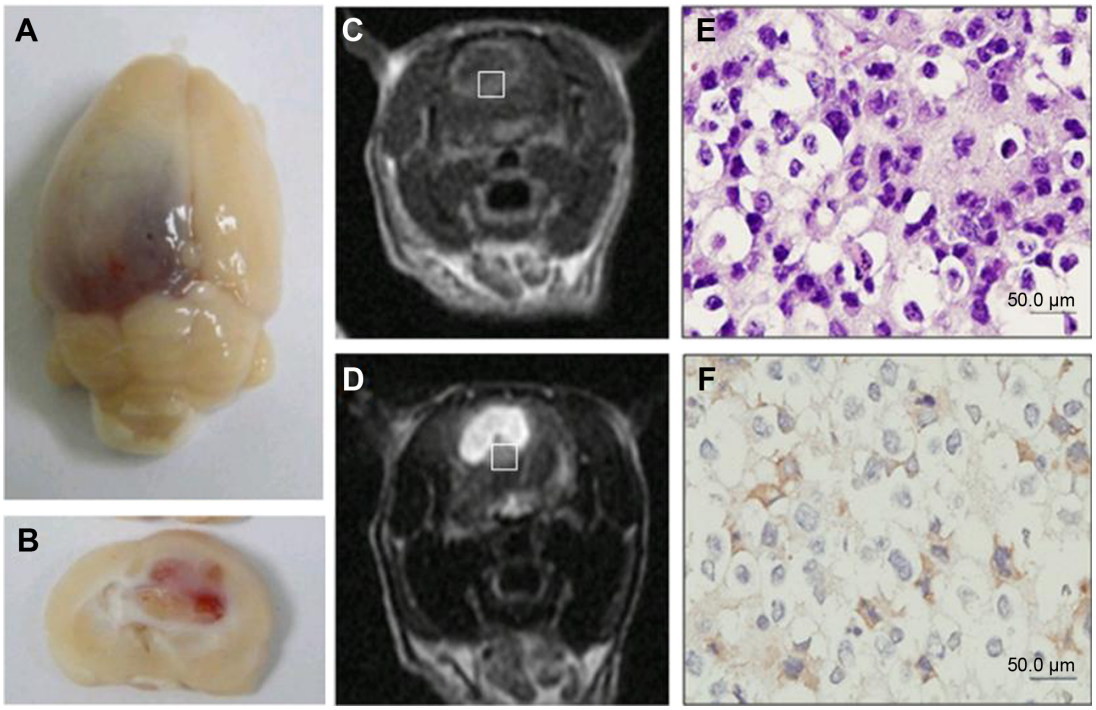

Figure S7 MR Images of ENU-induced rat brain tumor. Gross images of brain tumor specimens (top view [**A**] and sectioned view [**B**]); T1- and T2-weighted MR images show an intracranial mass with cystic necrosis (T1-weighted MR image [**C**] and T2-weighted MR image [**D**]); H&E staining (**E**) and CD133 immunostaining (**F**) at 400× magnification in rat brain tumor.

Abbreviations: H&E, hematoxylin and eosin; ENU, *N*-ethyl-*N*-nitrosourea; MR, magnetic resonance.